AGU PUBLICATIONS

JGR

Journal of Geophysical Research: Oceans

RESEARCH ARTICLE

10.1002/2015JC011012

Special Section:
Forum for Arctic Modeling and Observational Synthesis (FAMOS): Results and Synthesis of Coordinated Experiments

On the flow of Atlantic water and temperature anomalies in the Nordic Seas toward the Arctic Ocean

L. Chafik[1,2], J. Nilsson[3], Ø. Skagseth[4], and P. Lundberg[3]

[1]NOAA/NESDIS Center for Satellite Application and Research, College Park, Maryland, USA, [2]Cooperative Institute for Climate and Satellites, University of Maryland, College Park, Maryland, USA, [3]Department of Meteorology and Physical Oceanography, Stockholm University, Stockholm, Sweden, [4]Institute of Marine Research and Bjerknes Centre for Climate Research, Bergen, Norway

Key Points:
- Simple dynamical measure from the SSH is developed
- Flow of Atlantic water into the Arctic is regionally controlled
- Warm anomalies propagate as response to an increase in the flow

Supporting Information:
- Supporting Information S1
- Movie S1

Correspondence to:
L. Chafik,
leon.chafik@noaa.gov

Citation:
Chafik, L., J. Nilsson, Ø. Skagseth, and P. Lundberg (2015), On the flow of Atlantic water and temperature anomalies in the Nordic Seas toward the Arctic Ocean, *J. Geophys. Res. Oceans*, *120*, 7897–7918, doi:10.1002/2015JC011012.

Received 2 JUN 2015
Accepted 3 NOV 2015
Accepted article online 5 NOV 2015
Published online 13 DEC 2015

Abstract The climatic conditions over the Arctic Ocean are strongly influenced by the inflow of warm Atlantic water conveyed by the Norwegian Atlantic Slope Current (NwASC). Based on sea surface height (SSH) data from altimetry, we develop a simple dynamical measure of the NwASC transport to diagnose its spatio-temporal variability. This supports a dynamical division of the NwASC into two flow regimes; the Svinøy Branch (SvB) in the southern Norwegian Sea, and the Fram Strait Branch (FSB) west of Spitsbergen. The SvB transport is well correlated with the SSH and atmospheric variability within the Nordic Seas, factors that also affect the inflow to the Barents Sea. In contrast, the FSB is influenced by regional atmospheric conditions around Svalbard and northern Barents Sea. Using a composite analysis, we further relate anomalous strong SvB flow events to temperature fluctuations along the core of Atlantic water. A warm composite anomaly is found to propagate northward, with a tendency to amplify enroute, after these events. A roughly 12 months delayed temperature signal is identified in the FSB. However, also in the Lofoten Basin interior a delayed temperature signal is found, which appears to originate from the NwASC. This study suggests that hydrographic anomalies both upstream from the North Atlantic, and locally generated in the Norwegian Sea, are important for the oceanic heat and salt transport that eventually enters into the Arctic.

1. Introduction

The seas bounded by Greenland, Iceland and Norway are commonly termed the Nordic Seas and represent 0.75% of the world-ocean surface area. Albeit their small area, they play a vital role in the global climate system [*Drange et al.*, 2005]. This is due to the inflow of warm and saline Atlantic water into the Nordic Seas, which is important for the production of dense water maintaining the cold equatorward limb of the Atlantic meridional overturning circulation [*Rahmstorf*, 1999; *Drange et al.*, 2005; *Hansen and Østerhus*, 2000], but also for the Arctic heat budget and sea-ice variability [*Koenigk and Brodeau*, 2014; *Årthun et al.*, 2012; *Polyakov et al.*, 2005; *Zhang et al.*, 1998].

The Nordic Seas are fed by warm and saline water from the Gulf Stream/North Atlantic Current as the upper limb of the meridional overturning circulation portrayed in Figure 1. The main heat conveyor of the Atlantic inflow through the Nordic Seas and toward the Arctic is the Norwegian Atlantic Slope Current (NwASC). This is a topographically steered current [*Aaboe and Nøst*, 2008; *Nøst and Isachsen*, 2003; *Isachsen et al.*, 2003] which traditionally has been measured at Svinøy by current meters [*Orvik and Skagseth*, 2003a; *Orvik and Niiler*, 2002; *Skagseth and Orvik*, 2002; *Orvik et al.*, 2001], but is thought to be coherent all the way to the Fram Strait [*Skagseth et al.*, 2004]. In this latter study, the current from the Irish-Scottish shelf to the Fram Strait was analyzed using geostrophic velocities estimated from satellite-derived sea-level anomalies, and it was found that the NwASC responds directly to the wind field over the Nordic Seas through Ekman dynamics. On interannual timescales, it has been found that the averaged wind-stress curl over the North Atlantic Ocean leads the Atlantic inflow at Svinøy by 15 months [*Orvik and Skagseth*, 2003b]. This suggests that on longer time scales the baroclinic response is also important [*Sandø and Furevik*, 2008]. However, this lag-relationship between the wind-stress-curl and warm water anomalies only proved to be valid during periods characterized by weak atmospheric forcing. During periods of strong atmospheric forcing, these warm water anomalies will extend deep into the mixed layer and follow *f*/*H* contours that do not connect to the

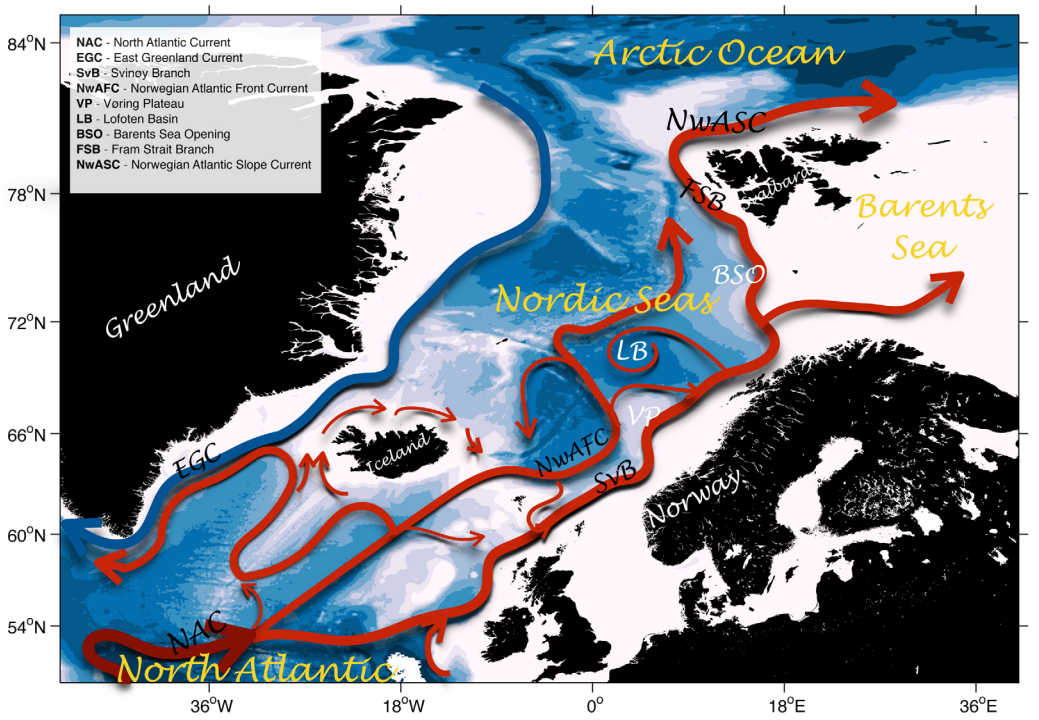

Figure 1. Map of the Nordic Seas including the bathymetry (shading) and a schematic representation of the large-scale pathways of Atlantic water in the northern North Atlantic and the Nordic Seas. Abbreviations in black denote current systems, and white denote regions. The focus of the present study is on the Norwegian Atlantic Slope current (NwASC); the main flow branch linking the North Atlantic to the Arctic and Barents Sea.

Nordic Seas. Thus it can be argued that the large year-to-year variations of the atmospheric circulation break down the predictability.

Strong and weak regimes of atmospheric forcing in the North Atlantic region are usually linked to the strength of the prevailing westerly winds as measured by the meridional mean sea-level pressure gradient between the Icelandic low and the Azores high quantified by an index termed the North Atlantic Oscillation (NAO); the leading mode of atmospheric variability in the North Atlantic [*Hurrell*, 1995]. During its positive phase, the westerlies are stronger than average, leading to more intense storms. However, during a negative NAO phase, the winds are weaker and there is a shift of the storm tracks southward [*Hurrell*, 1995]. Generally, these shifts are associated with north-south migrations of the jetstream [*Woollings et al*., 2010].

The ocean-climate variability in the Nordic Seas has frequently (see the review by *Furevik and Nilsen* [2005, and references therein]) been investigated based on the relationship of the warm water inflow and its connections to the NAO [*Richter et al*., 2012; *Furevik*, 2001; *Mork and Blindheim*, 2000]. The latter investigators found that on interannual timescales, variations of volume transport, temperature and salinity at Svinøy are positively correlated with the NAO index. *Richter et al*. [2009] demonstrated that the activity, intensity and residence time of cyclones in the Nordic Seas are important factors for interannual transport anomalies. Using a linear regression model, *Richter et al*. [2012] were able to reconstruct the transport variability back to the 1960s, and showed that the NAO is responsible for the variability of the Svinøy transport. Whether this covariability holds downstream remains to be investigated. However, *Lien et al*. [2013] show, using a numerical model, that atmospheric circulation in the northern Barents Sea may influence the extension of the NwASC flowing west of Spitsbergen toward the Fram Strait (here termed Fram Strait Branch or FSB, cf. Figure 1).

The heat content of Atlantic water in the Nordic Seas varies over seasonal to decadal timescales [*Yashayaev and Seidov*, 2015; *Mork et al*., 2014; *Chepurin and Carton*, 2012; *Carton et al*., 2011; *Furevik*, 2001]. The cause of this variability has been linked to both air-sea heat fluxes and advective processes. *Yashayaev and Seidov* [2015] show that Nordic-Seas heat content anomalies correlate well with the low-frequency variability of the NAO and the Atlantic Multidecadal Oscillation, i.e., the averaged sea surface temperature in the North

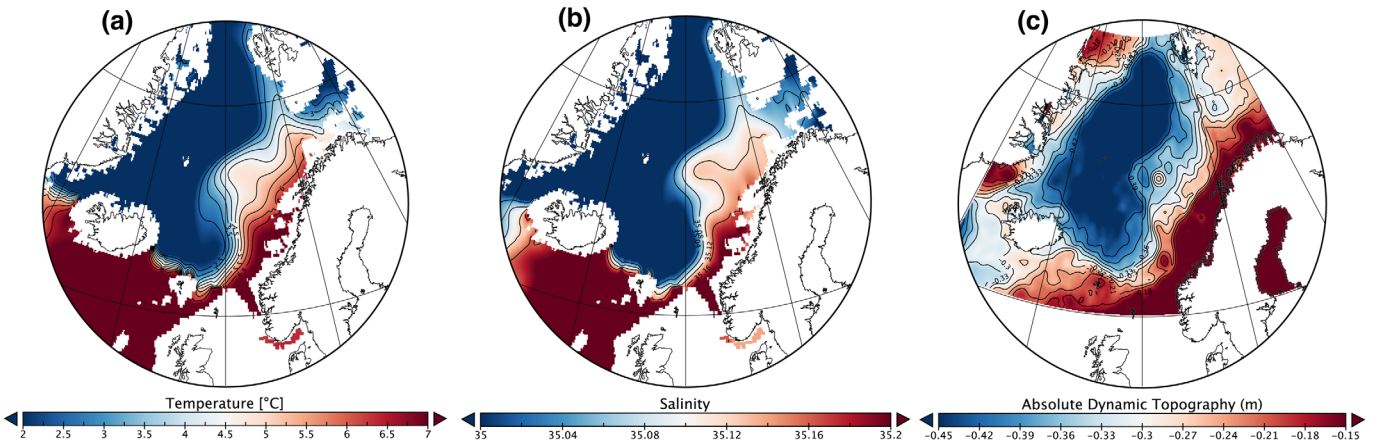

Figure 2. Distribution of Atlantic water in the Nordic Seas. The ~300 m (a) temperature and (b) salinity fields are from the 2013 high-resolution (0.25° × 0.25°) Nordic Seas regional climatology [*Seidov et al*., 2015]. (c) The time mean (1992–2012) Absolute Dynamic Topography. A large fraction of the warm Atlantic water branches into the Barents Sea, complicating the continuation toward the Fram Strait. A tongue of warm and saline Atlantic water and high Absolute Dynamic Topography is seen to extend into the interior of the Lofoten Basin.

Atlantic. *Skagseth and Mork* [2012] show an increasing trend of ocean heat content in the Nordic Seas, and argue that the main mechanism is advection of heat from the North Atlantic due to the weakening of the subpolar gyre and the associated northward penetration of subtropical water [*Häkkinen et al*., 2011; *Hátún et al*., 2005; *Häkkinen and Rhines*, 2004]. Most recently, *Mork et al*. [2014] have shown that air-sea heat fluxes can explain about 50% of the interannual variability of the Norwegian-Sea heat content. In contrast, *Carton et al*. [2011] demonstrate that the net surface heat flux is not a dominant factor. Instead, they suggest anomalous advection of Atlantic Water into the Nordic Seas as the more plausible explanation. It is likely that both air-sea fluxes and advective processes control the hydrographic anomalies in the Nordic Seas. We here explore an alternative mechanism, i.e., whether warm anomalies in the Nordic Seas could also be caused by an increase of the northward flow in the southern Norwegian Sea (here termed the Svinøy branch or SvB, cf. Figure 1), rather than by advection of" warm packets" from the North Atlantic, a mechanism proposed by *Sundby and Drinkwater* [2007].

The Nordic Seas bathymetry plays an important role for steering the flow of Atlantic water toward the Arctic region [*Koszalka et al*., 2011; *Søiland et al*., 2008; *Isachsen et al*., 2003; *Orvik and Niiler*, 2002; *Poulain et al*., 1996], but also for the eddy-mean flow interaction. Recent research focusing on the circulation of the Nordic Seas has also been directed toward estimating the mean flow and its associated eddy activity using a large number of intermediate-depth floats [*Rossby et al*., 2009a] and surface drifters [*Andersson et al*., 2011; *Koszalka et al*., 2011, 2013]. For drifters moving from the southern Norwegian Sea to the Barents Sea Opening (BSO), *Koszalka et al*. [2013] quantified the transit time to be around 200 days, but also noted that the span of arrival times ranged from months to years. In addition, these drifters spent almost half their journies, i.e., around 100 days, trapped within the Lofoten Basin (LB). According to *Björk et al*. [2001] this region, apart from being the major heat reservoir in the Nordic Seas (note the spread of Atlantic water into the LB in Figure 2), is also characterized by eddies originating from the NwASC [*Raj et al*., 2015; *Köhl*, 2007]. However, it is as yet unclear whether these eddies transfer hydrographic anomalies into the LB interior.

We start by describing the altimetric, hydrographic and atmospheric data sets used in this study. This is followed by a dynamical background, a sensitivity analysis of our altimetrically derived NwASC measure, and a validation against current-meter data. The results section focuses on (i) the spatio-temporal variability and consistency of the NwASC flow, (ii) identifying the monthly and interannual atmospheric and sea-surface height patterns associated with the SvB and FSB flow variability, and (iii) propagation of hydrographic anomalies toward the Fram Strait and into the LB respectively. The results are discussed in section 7. Concluding remarks ends the paper.

2. Data Set Description

2.1. Satellite Altimetry

The sea-surface heights (SSHs) used in this study are based on the globally gridded (1/3° ×1/3°) and Mercator-projected absolute dynamic topography at weekly resolution (provided by AVISO). This weekly

data set from October 1992 to December 2012 is temporally averaged to form monthly fields. We use the reference product of the SSH, i.e., two satellites orbiting the same groundtrack over the entire sampling period, to ensure that the sampling was stable in time during the analysis period. Note that the SSH is a combination of the sea-level anomalies (SLAs) and the ocean mean dynamic topography [*Rio et al*., 2011], which in turn is based on a number data sets: the GRACE (Gravity Recovery and Climate Experiment) geoid, an altimetric Mean Sea Surface as well as altimetric SLAs, wind-stress data and oceanographic in situ data. By combining these data sets, *Rio et al*. [2011] showed that an improved marine geoid was obtained, and thus the SSH now yields a better consistency with independent *in-situ* measurements. For the Nordic Seas, *Volkov and Pujol* [2012] provided a comprehensive validation study of the gridded satellite altimetry, and showed that this can be successfully used to study the variability of sea-level and surface geostrophic velocities in the region.

2.2. Hydrographic Data

We use the recently published high-resolution regional (Nordic and Barents Seas) hydrographic data produced by the National Oceanographic Data Center [*Seidov et al*., 2015; *Korablev et al*., 2014]. It is a compilation of all available data (37 different) sources for the area bounded by 60–82°N, 40–70°E [*Korablev et al*., 2014]. To our knowledge, it is the only database that merge all available oceanographic measurements into one single database. All duplicates were removed using automatic algorithms as well as expert visual control. It should also be emphasized that the Atlas used original data that has not been subjected to any interpolation in the vertical. Doing so, it is insured that the same uniform interpolation algorithm is used. The spatial resolution is $0.25^\circ \times 0.25^\circ$ with a monthly temporal resolution. An interpolation algorithm has been developed specifically to interpolate the unevenly distributed observation into the regular grid. The technique is referred to as Data-Interpolating Variational Analysis or DIVA, and particularly suited for interpolating unevenly spaced and noisy data [*Troupin et al*., 2012]. One main advantage of this method, which rely on a finite-element resolution, is that it actually takes into account topographic as well dynamic constraints, such as coasts, subbasin and advection. The data have been extensively checked for quality and biases arising from instruments were all eliminated from the data used in this hydrographic Atlas. Between 1992 and 2012, which is the time period under consideration here, about 60.000 temperature profiles have been compiled in the Nordic Seas. *Seidov et al*. [2015] state that in the Nordic Seas, both temperature and salinity can be reconstructed on a quarter-degree grid with relatively high confidence. The data density in the Nordic Seas is good with more than 10 stations within each quarter-degree gridbox for the annual period. In the present study, we only use the temperature field following the main core of Atlantic Water (supporting information Figure S1), which has been de-seasoned by removing the annual cycle and linearly detrended in order to compute the anomalies.

2.3. Atmospheric Data

We use the ERA-interim reanalysis [*Dee et al*., 2011] provided by the European Centre for Medium-range Weather Forecasts. The field retrieved is the Mean Sea Level Pressure (MSLP) from 1992 to 2012 with a horizontal resolution of $1^\circ \times 1^\circ$. The monthly means used here are temporally averaged from daily means. The monthly MSLP has also been de-seasoned by removing the annual cycle and linearly detrended.

3. Measuring the NwASC From Altimetry

3.1. Dynamical Background

As an altimetrically based dynamical indicator of the NwASC at time t, we will use the difference in absolute dynamic topography between the 500 and 900 m isobaths (shown in supporting information Figure S2). At each point along this current, denoted by the coordinate s, the height difference in the direction normal to the isobaths is calculated as

$$\Delta_H \eta(s,t) \equiv \eta(H_{500},s,t) - \eta(H_{900},s,t), \tag{1}$$

where η is the dynamical topography. From the geostrophic balance

$$\mathbf{u} = (g/f)\mathbf{k} \times \nabla \eta, \tag{2}$$

where $\mathbf{u}$ is the horizontal velocity, g the acceleration of gravity, f the Coriolis parameter and $\mathbf{k}$ the vertical unit vector, it is found that

$$\int_{n(H_{500})}^{n(H_{900})} \mathbf{u}\cdot\mathbf{s}\,dn=(g/f)\Delta_H\eta(s,t), \tag{3}$$

where n is a coordinate normal to the isobaths and $\mathbf{s}$ a unit vector along the isobaths, directed with shallow water to the right. Accordingly, $\Delta_H\eta(s,t)$ is proportional to the integrated geostrophic surface velocity between the isobaths.

If the flow is equivalently barotropic, implying that the velocity changes magnitude but not direction with depth, then, following *Killworth* [1992] and *LaCasce and Isachsen* [2010], it can be stated that

$$\mathbf{u}(x,y,z,t)=(g/f)\mathbf{k}\times\nabla\eta(x,y,t)\,P(z), \tag{4}$$

where $P(z)$ is a nondimensional function describing the vertical pressure variation with the property $P(z=0)=1$. Under this assumption, it is straightforward to show that the volume transport between two isobaths is given by

$$\int_{n(H_1)}^{n(H_2)}\int_{-H}^{0}\mathbf{u}\cdot\mathbf{s}\,dzdn=-\int_{H_1}^{H_2}\frac{\partial\eta}{\partial H}\mathcal{H}(H)\,dH \tag{5}$$

where we have introduced

$$\mathcal{H}(H)\equiv\int_{-H}^{0}P(z)\,dz. \tag{6}$$

Note that in the purely barotropic case, $P(z)=1$ and $\mathcal{H}=H$. The transport between the 500 and 900 m isobaths can, in the equivalently barotropic case, to leading order be calculated as

$$\Psi(s,t)=(g/f)\Delta_H\eta(s,t)\mathcal{H}(H_{700}), \tag{7}$$

where H_{700} is the arithmetic mean of the isobath range. Thus, for barotropic or equivalently barotropic flow, the NwASC volume transport between the 500 and 900 m isobaths should thus approximately be proportional to $\Delta_H\eta(s,t)$. However, as $\Psi(s,t)$ is proportional to integrated geostrophic surface velocity between the isobaths, it can simply be interpreted as an along-stream dynamical measure of the NwASC.

3.2. The Transport Proxy: Sensitivity Analysis and Validation

Figure 3 illustrates $\Psi(s,t)$ and its variability along the NwASC. To begin with, we initially note that the time-mean Ψ varies along the NwASC path, which is not to be expected if the flow to be equivalently barotropic. This indicates that the time-mean Ψ signal contains additional dynamics such as baroclinic flow or reflects errors, e.g., in the geoid estimate; an issue which will be discussed later. Focusing on the time-dependent part of $\Psi(s,t)$, we note that the variance of this quantity changes along stream and tends to be correlated with the bottom slope (see supporting information Figure S2). To examine the correlation between the time-dependent part of $\Psi(s,t)$ and the NwASC volume transport, we compare our altimeter-derived transport proxy $\Psi(s,t)$ with in situ current-meter based transport estimates from the Svinøy section [*Orvik et al.*, 2001; *Orvik and Skagseth*, 2003a]. The latter show that one single current moored current meter is capable of monitoring the Norwegian Atlantic slope current. The current meter series used here is accordingly an index series based on one single current meter and instrument depth located at a depth of 100 m at 63°N, 4°E over the 500 m isobath. As our proxy of the NwASC transport is limited to the difference in the SSH between the 500 and 900 m isobaths, we examine its sensitivity to the choice of the outer isobath. Figure 4 shows the relationship between the current-meter based transport and the altimeter-derived transport proxy for different outer isobaths. The diagonal (broad) shape characterizing the results in Figure 4 indicates that the correlation is stronger (weaker) for isobaths less-or-equal to (greater than) 1000 m. However, the largest number of occurrences along the identity diagonal is found using the 900 m isobath (Figure 4b). This is used in Figure 5, where we underline that this simple measure captures the current-meter transport estimates in the Svinøy section reasonably well (with a correlation of ~0.66). This suggest that the time-varying flow in the Svinøy section is approximately equivalently barotropic, i.e., the transport variability is proportional to the cross-slope surface height difference between 500 and 900 m isobaths. Is it, however, possible to assume that this is the case also downstream? As shown by supporting information Figure S3, we also find a reasonably good agreement in the time variability between current-meter data from Gimsøy and Bjørnøya and our transport proxy from altimetry.

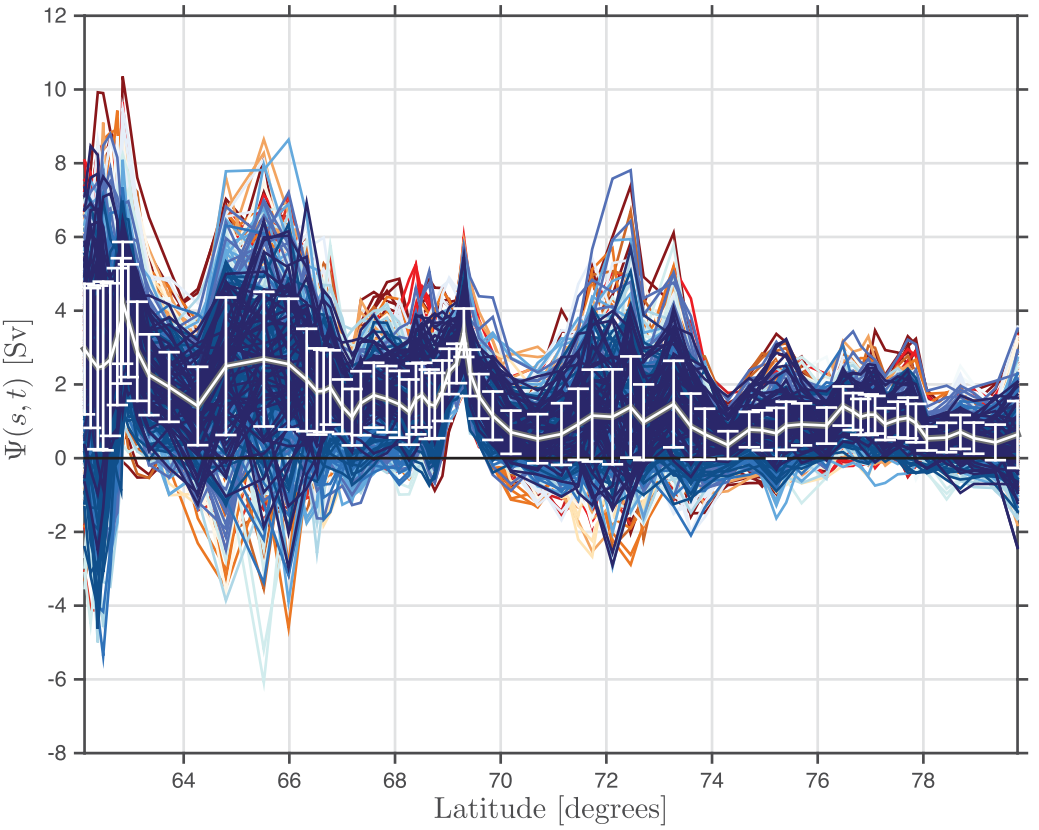

Figure 3. The transport proxy along the NwASC as a function of latitude. The thin colored lines represent the raw (neither de-seasoned nor detrended) weekly transport between 1992 and 2012. The grey line is the time-mean transport and the associated vertical bars indicate the spread. Note that due to baroclinic effects the time mean "barotropic" transport varies along-stream. However, the time-dependent transport fluctuations tend to be essentially barotropic (cf. Figure 5 and supporting information Figure S3).

4. Spatiotemporal Variability of the NwASC

In this section, we resolve the spatio-temporal variability of the NwASC from 62°N up to 80°N. This approach permits us to explore how transport variations at a specific location covary with the entire NwASC. In particular, we investigate the immediate NwASC behavior to variations of the SvB and FSB; the main conduits of heat and salt in the Nordic Seas and into the Arctic Ocean [*Beszczynska-Möller et al.*, 2012; *Polyakov et al.*, 2005; *Poulain et al.*, 1996]. In addition, a lag-analysis is applied to identify signals propagating through the system.

4.1. How Consistent Is the NwASC?

We now investigate the spatial consistency of the NwASC. In particular, we examine how changes of the SvB and FSB project onto the entire current. This is based on a correlation analysis of our NwASC flow measure, estimated according to:

$$R(s)=\frac{\sum_{n=1}^{N}\bar{\Psi}_{seg}(t)\cdot\Psi(s,t)}{\sqrt{\sum_{n=1}^{N}\bar{\Psi}_{seg}(t)\cdot\bar{\Psi}_{seg}(t)}\sqrt{\sum_{n=1}^{N}\Psi(s,t)\cdot\Psi(s,t)}}, \tag{8}$$

where the summation is over the entire observation period of the deseasoned monthly transports. This type of analysis typically results in a high correlation $R(s)$ over the base segment $\Psi_{seg}(t)$ itself (i.e., SvB or FSB), and varying correlation coefficients elsewhere. Since our focus is on the large-scale variability of the SvB/FSB, it is noteworthy that the along-stream segment-averaging is done to reduce the effect of small-scale variability that contaminates a single point.

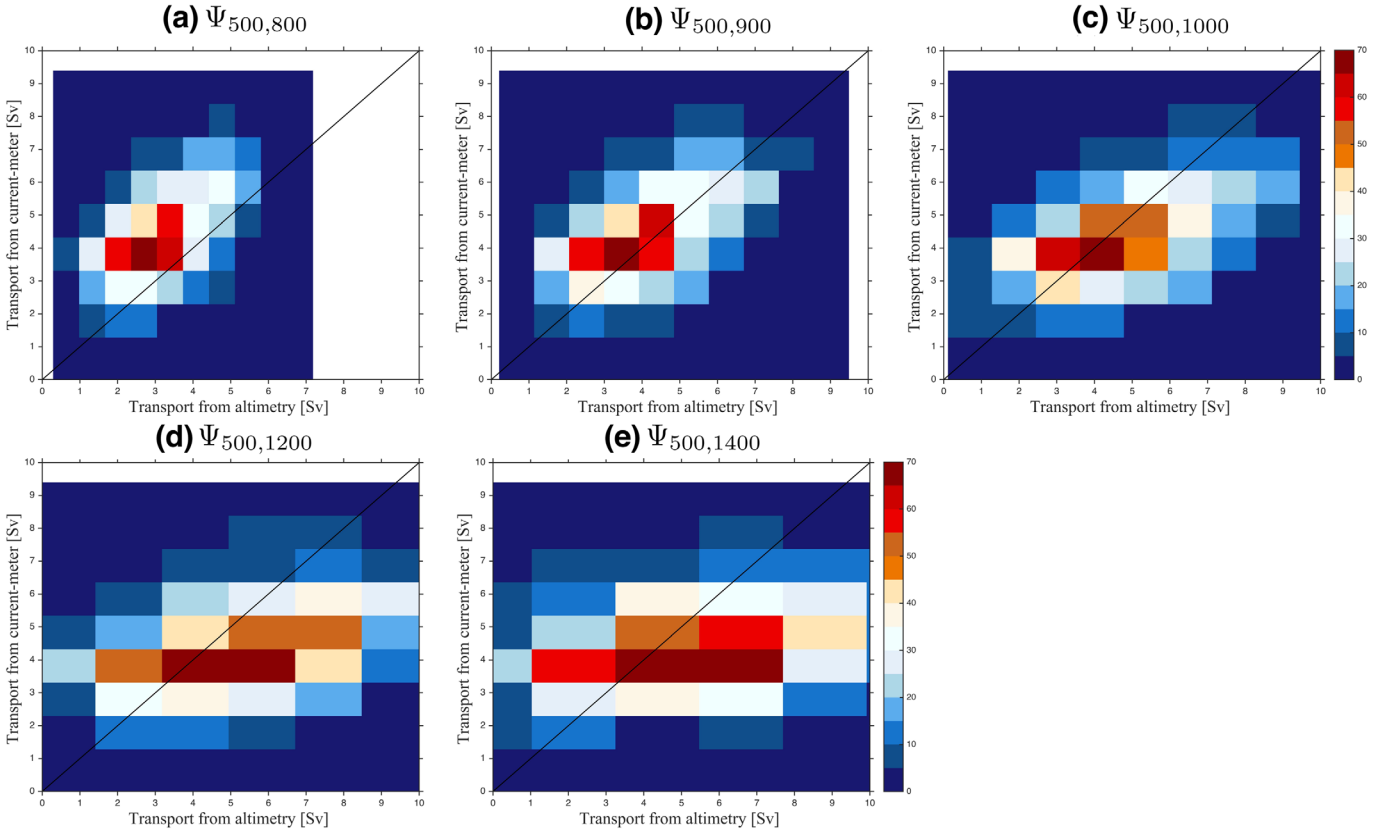

Figure 4. Two-dimensional histograms of the weekly distributions of the Svinøy current-meter (deployed at a depth of 100 m) transport versus the altimeter-derived transport proxy (in $Sv=10^6\ m^3s^{-1}$) at a point near Svinøy using five different outer isobaths, *viz*. (a) 800 m, (b) 900 m, (c) 1000 m, (d) 1200 m, and (e) 1400 m. The time series are neither de-seasoned nor detrended. The current meter series used here is an index series based on one single moored current meter located at a depth of 100 m at 63°N, 4°E over the 500 m isobath [*Orvik and Skagseth*, 2003a]. The largest number of occurrences along the identity diagonal is found using the 900 m outer isobath (Figure 4b), which we hence choose for constructing our along-stream dynamical measure of the NwASC, i.e., $\Psi(s,t)$.

Figure 6 illustrates the along-stream correlation pattern based on the SvB/FSB transport time series. Figure 6a reveals that the correlations are high along the SvB segment itself (R ∼0.8) but also along part of the Lofoten escarpment (R ∼0.5–0.6). The weakest correlations are over VP (R ∼0.3–0.4), BSO and FSB (R ∼0.2–0.4). Figure 6b shows, as expected, a high correlation along the FSB, and a slow but sustained decrease of the correlation coefficient down to ∼70°N. Further south, i.e., along the Norwegian continental slope, a more-or-less homogeneous relationship explaining only about 5–15% (cf. Figure 6c) is seen to dominate. Note that the SvB curve (red line) shows a more rapid decline as compared to the FSB (blue line), but also explains about 5–15% north of 70°N. In the next section, we explore how the flow behaves at lead times up 24 months.

4.2. Memory of the Poleward Flow

Figure 7 show the lagged response of the NwASC to anomalous positive barotropic flow in the SvB. We note in the zero-lag results, as previously shown in terms of correlation, that positive anomalies dominate the NwASC, but with damped magnitudes north of the Lofoten slope (∼70°N) and along the FSB. This positive anomaly in the flow (at zero lag) is most likely due to the strong topographical steering, which is consistent with the anticipated increase of the wind-driven barotropic flow along f/H contours (H being the depth) in the Nordic Seas [*Isachsen et al*., 2003; *Nøst and Isachsen*, 2003]. The signal continues to show positive anomalies 4–5 months, especially at Svinøy and Lofoten (note that this not the case at around 66°N, i.e., the VP), after an anomalous transport at Svinøy. Whilst, along BSO and FSB the signal vanishes immediately after the zero-lag. After 12–16 months, we observe that a negative transport signal once again dominate Svinøy and Lofoten. The reason for this anomaly to appear after 1 year is not immediately evident to us, but could be related to the prominent year-to-year hydrographic changes in the Atlantic water driven by the local atmospheric heat fluxes reported by *Mork et al*. [2014]. Clearly, a signal due to an increase of the

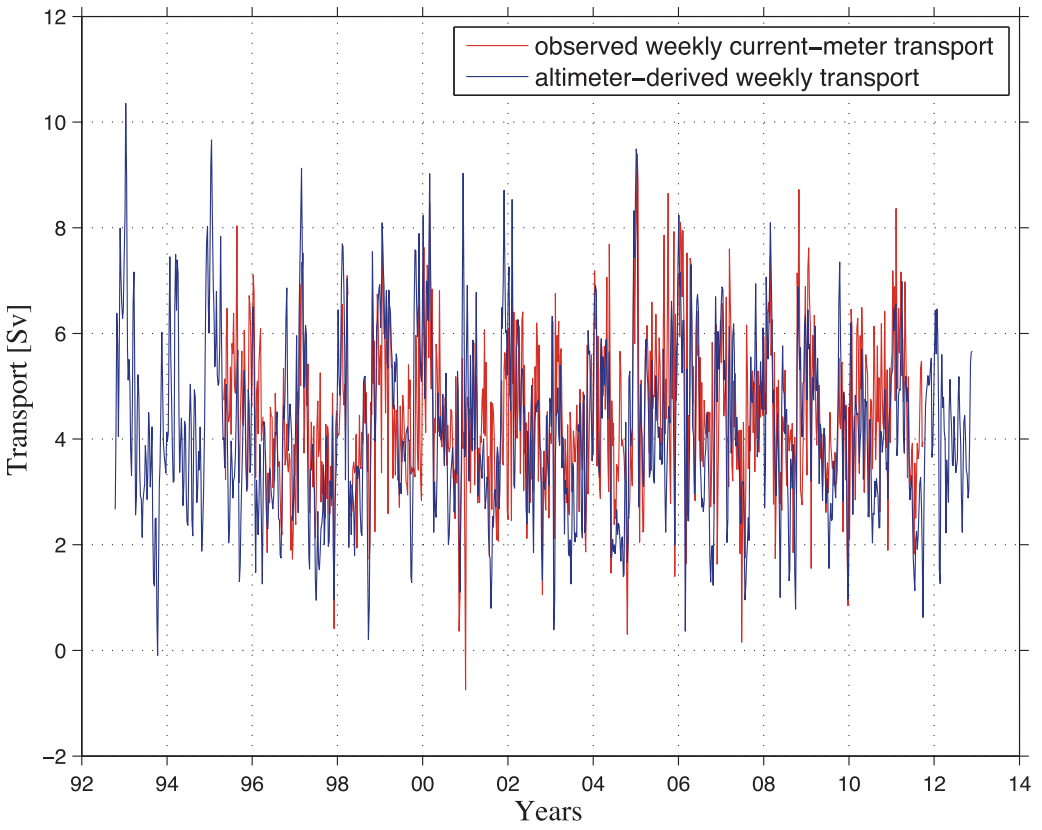

Figure 5. Comparison of the weekly averaged current-meter transport from Svinøy (1995–2011) and the weekly altimeter-derived transport 1992–2012 (based on the 500–900 m isobath, cf. Figure 4b) from a point close to the Svinøy station. The time series are neither deseasoned nor detrended. The current meter series used here is an index series based on one single moored current meter located at a depth of 100 m at 63°N, 4°E over the 500 m isobath [*Orvik and Skagseth*, 2003a]. The time-mean estimates and the standard deviations are approximately 4.4 ± 1.4 Sv and 4.2 ± 1.7 Sv for the current-meter data and the altimetry, respectively. The fact that the two measurements are comparable (correlation coefficient of ∼0.66 at the 99% confidence level) suggests that our transport proxy is reasonable.

transport in the southern Norwegian Sea has longer memory in the vicinity of Svinøy and Lofoten, but is lost immediately after the zero-lag at the BSO and FSB.

5. Atmospheric Forcing and Oceanic Pressure Field on Monthly to Interannual Scales

Here we aim at identifying the SSH/MSLP spatial patterns that can explain most of the SvB and FSB variability. This analysis is conducted on monthly and interannual timescales. Since the variability of the circulation in the Nordic Seas is largely wind-driven, i.e., increases/decreases of the winds lead to a spin up/down of the NwASC [*Richter et al*., 2012; *Aaboe and Nøst*, 2008; *Skagseth et al*., 2004; *Skagseth*, 2004]. Hence the SvB and FSB should in theory reflect similar circulation patterns. However, we learn that the SSH/MSLP patterns driving the SvB are distinctively different from that of the FSB, especially on interannual timescales.

5.1. Corresponding SSH Patterns

Figure 8 shows that the correlation pattern of the SSH field is consistent with a surface flow in geostrophic balance: the transports in both SvB and FSB tend to be high when SSH is elevated in the coast to shelf-edge zone and depressed in the central basin. The SSH correlation pattern in the Barents Sea is slightly different but also compatible with geostrophic dynamics. This quasi-steady along-isobath SSH transition has also been interpreted as a lower-mode continental shelf wave [*Gordon and Huthnance*, 1987]. However, on interannual timescales the SSH within the Nordic Seas shows a stronger negative correlation (more depressed SSH), while the positive correlation along the coast and in the Barents Sea vanishes completely. For the FSB, it is seen that on monthly timescales, a strong positive correlation exists along the coast of Norway and in

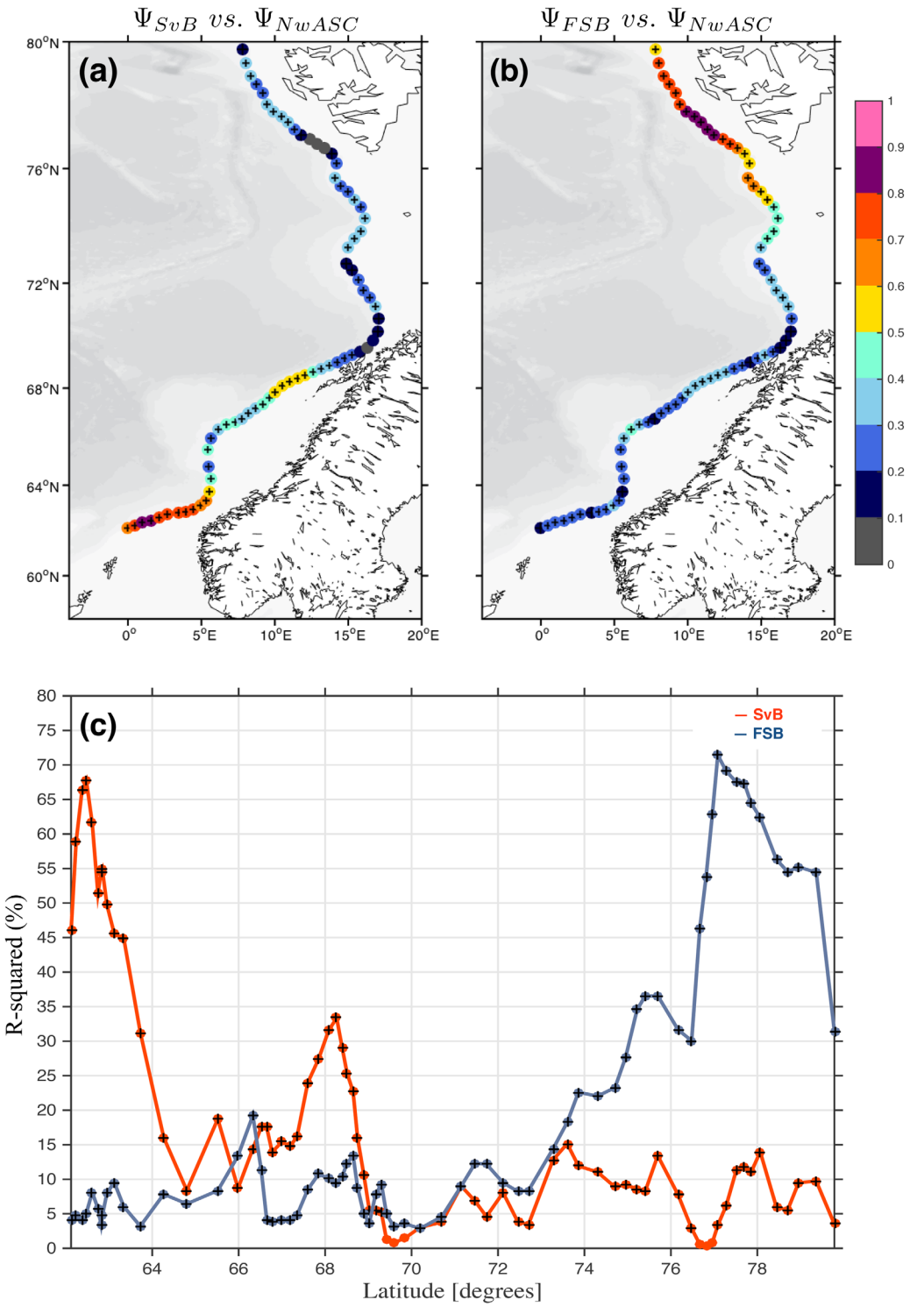

Figure 6. Correlation between monthly transport proxy anomalies at the (a) SvB, and (b) FSB versus and along the entire NwASC (Ψ_{NwASC}). (c) The squared correlation coefficient (R-squared, in %) of the SvB (Figure 6a) and FSB (Figure 6b) correlation structures. The de-seasoned and detrended data transport proxy data are used to compute the anomalies. A plus sign inside a circle indicates that the correlation is significant at the 95% level ($p < 0.05$). The covariability with the NwASC is weak north/south of 70°N for the SvB/FSB.

the Barents Sea (note the northward shift of the maximum correlation in the Barents Sea as compared to the results based on SvB transports), while the negative correlation within the Nordic Seas is weak. This suggests that the flow along the FSB is mainly driven by the high SSH originating in the Barents Sea and less so

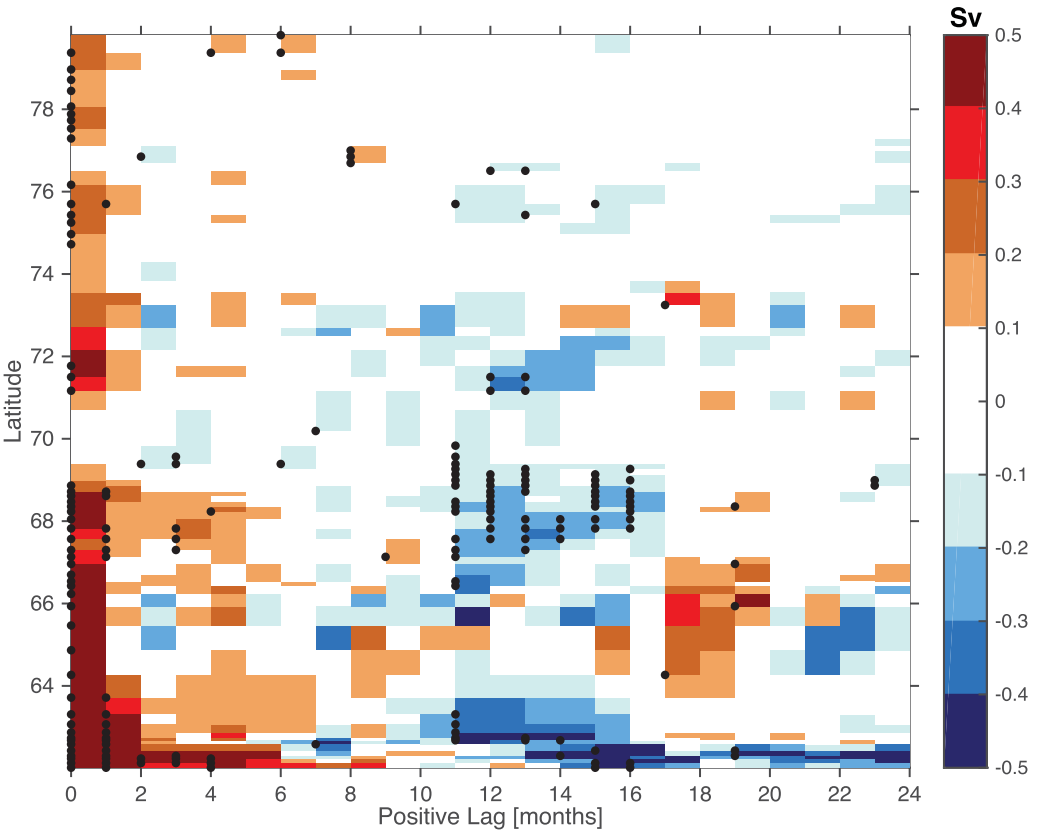

Figure 7. Time lag composite analysis (time-latitude) of the monthly transport proxy anomalies, in *Sv*, along the NwASC. The composite is based on anomalous SvB monthly transport events, defined as months exceeding 1 standard deviation. Positive lags are evaluated up to 24 months. Black stipplings represent grid points that are significant at the 95% confidence level ($p < 0.05$) assessed based on a two-sided t-test. Reduced transport anomalies are found north of ~70°N, while the memory of the flow appears to be prolonged at Svinøy and Lofoten.

by the depressed SSH within the Nordic Seas. On interannual timescales, the positive correlation surrounding Svalbard becomes more distinct, suggesting that a regional pattern connected to the Barents Sea is driving the flow along the FSB [*Lien et al.*, 2013]. One possible interpretation is that the FSB transport-proxy variability on interannual timescales reflects a fractionation of the Atlantic Water transport toward the Arctic between the Fram Strait and Barents Sea branches, which is presumably controlled by regional wind conditions around Svalbard; a notion supported by the analysis of the atmospheric circulation patterns presented below.

5.2. Large-Scale or Regional Atmospheric Forcing?

The large-scale MSLP correlation patterns show, on both short and long time scales, that the SvB variability (Figures 9a and 9b) is anti-correlated with the pressure field; hence the cyclonic wind circulation within the Nordic Seas. On monthly timescales, the maximum and minimum correlation coefficients display a tilted orientation, leading to enhanced southwesterlies parallel to the Norwegian coast, a divergence of the wind-induced Ekman transport and a spin-up of the circulation. On longer time scales, the large-scale pattern of the MSLP continues to be NAO-like, but the correlation minimum has shifted within the Norwegian Sea, suggesting that the wind field here may play a role on longer time scales. The FSB, however, shows a different atmospheric pattern, especially on interannual timescales but also on monthly timescales. Figure 9c shows that the minimum correlation has shifted westward, weakened significantly and become confined to the Nordic Seas. It does not extend into the Barents Sea as in the SvB case. On longer time scales, the FSB shows a significant positive correlation encircling Svalbard and northern Barents Sea, consistent with the SSH pattern in Figure 8d. This resulting positive MSLP anomaly induces an increase in the SSH and hence an anticyclonic circulation anomaly, which enhances the flow along the FSB.

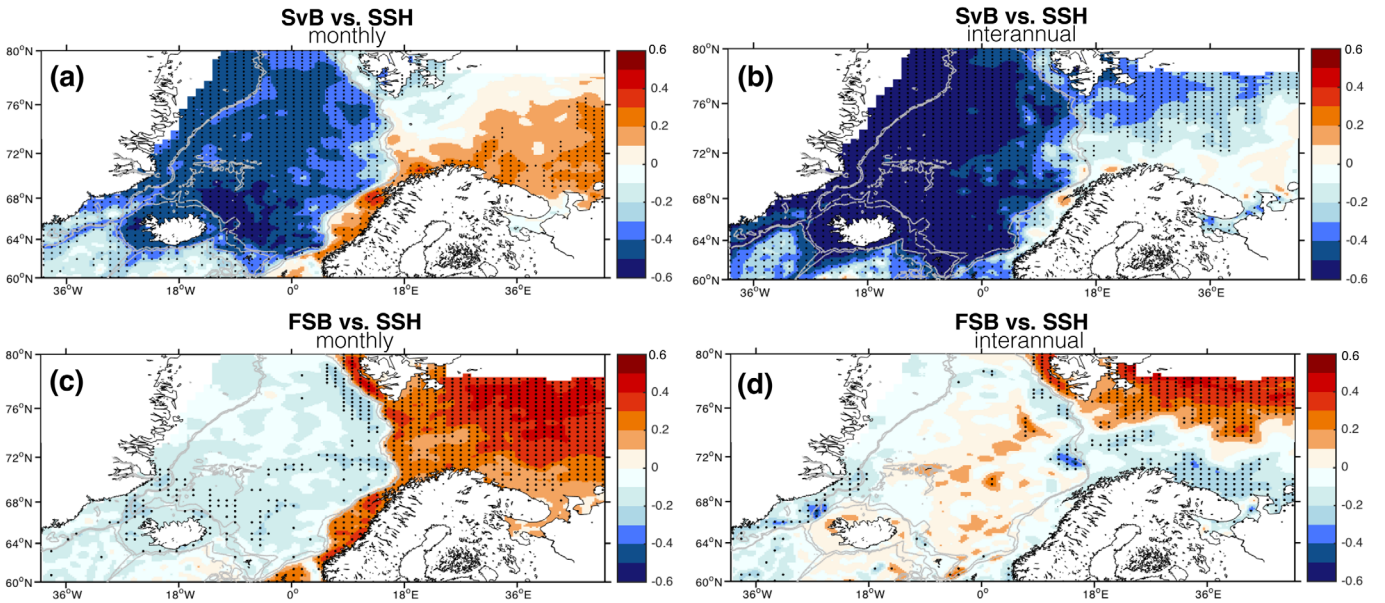

Figure 8. Correlation of the SvB/FSB monthly transport proxy anomalies and the SSH anomaly (de-seasoned and detrended) on (a, c) monthly (no-filtering), and (b, d) interannual timescales (1 year running mean). Black stipplings represent grid points that are significant at the 95% confidence level ($p < 0.05$) assessed based on a two-sided t test. The SSH anomaly within the Nordic Seas and over the Northern Barents Sea appears to be important for the SvB and FSB, respectively.

It is evident that on interannual timescales the strength of the cyclonic circulation anomaly within the Nordic Seas is dynamically irrelevant for the FSB, and that the SvB is driven by a modified NAO pattern. This is further investigated in Figure 10, which shows the cross-correlation between the NAO, the SvB and FSB on interannual timescales. It is evident that the NAO is not the driving mode for the FSB. The regional circulation identified above is the dominant forcing mechanism. And that even if the atmospheric circulation driving the SvB is of NAO type, their covariability is low and nonsignificant at zero-lag. Presumably, since the nodes of the atmospheric low and high are misplaced, the traditional NAO index is not applicable. However, we find a significant maximum lag-correlation of 0.36 at 9 months, i.e., the NAO leads the SvB by 9 months on interannual timescales. A mechanism that may be relevant when considering longer time scales is that of *Blindheim et al*. [2000]. The latter investigators found that the westward extent of Atlantic Water in the Norwegian Sea decreased as an integrated response to positive NAO conditions. They interpreted this as the Norwegian Atlantic Current being more confined to the continental slope by affecting its lateral extent, and our result showing that positive NAO leads the NwASC on interannual timescales is in accordance with this interpretation.

6. Poleward Propagating Warm Temperature Anomalies

We here investigate whether temperature anomalies propagating toward the Fram Strait (an obvious pathway consistent with the general ocean circulation of the Nordic Seas) and into the LB are generated as a response to an increase in the SvB transport. The analysis concerning anomalies propagating into the LB is performed since we note that the correlation (SvB versus NwASC, cf. Figure 6a) is significantly reduced downstream of the Lofoten slope. We hypothesize that this reduction may be due, but not limited (reasons to be discussed later), to the vigorous cross-slope eddy shedding here [*Isachsen*, 2015; *Raj et al*., 2015; *Jakobsen et al*., 2003]. To support this conjecture, the slope-to-basin propagation of temperature anomaly is studied.

6.1. Toward the Fram Strait

Figure 11 shows the evolution of composite temperature anomalies along the NwASC following an increased SvB transport. At zero lag, we observe a temperature anomaly (nonsignificant at the 95% confidence level) at depth between 300 and 600 m. The core of this warm anomaly appears in the vicinity of Lofoten already after 2 months (at a depth of ∼100 m), but the warm area stretches from the VP to Lofoten.

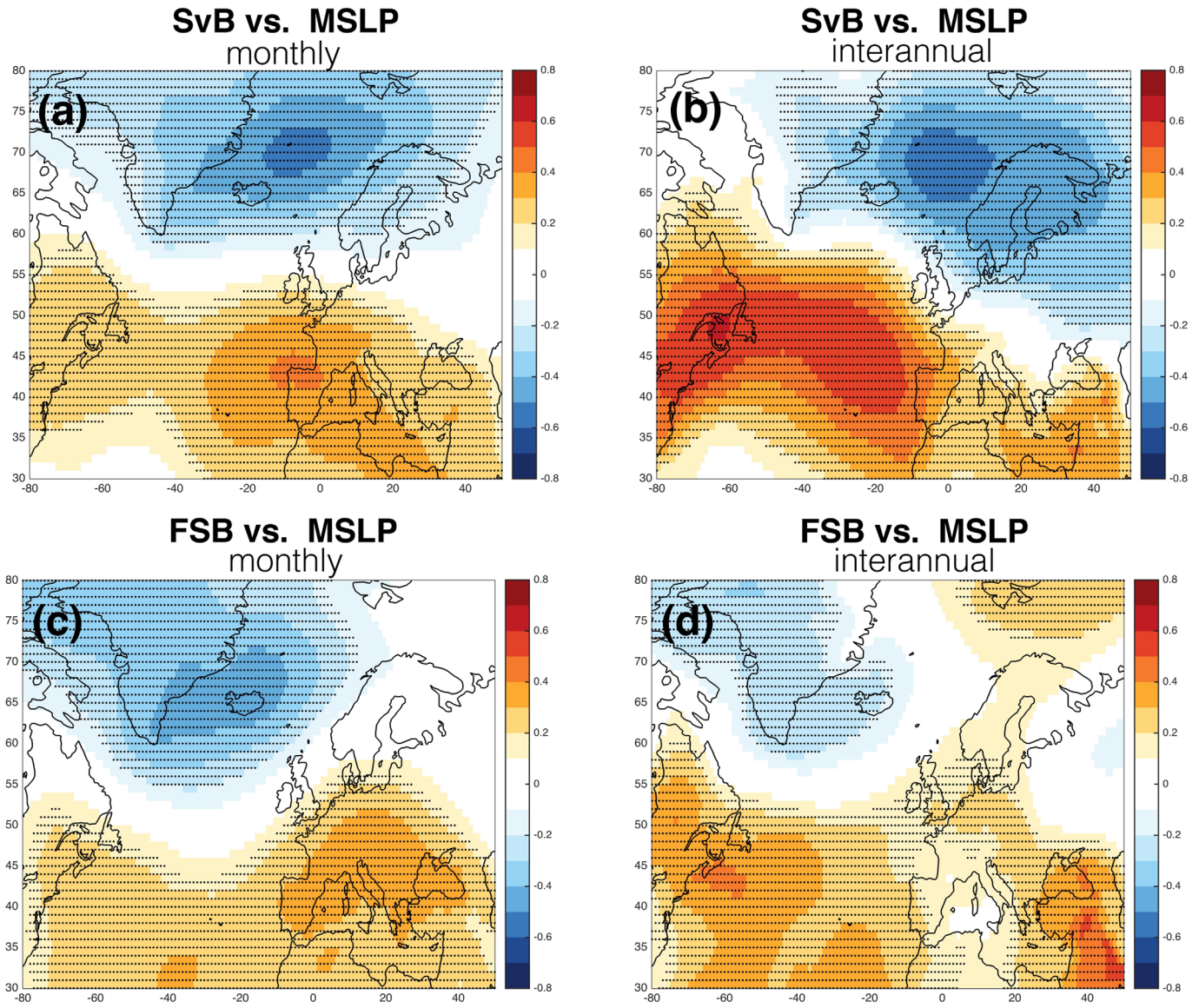

Figure 9. Same as Figure 8 but for the MSLP anomaly (de-seasoned and detrended). The SvB can be associated with MSLP within the Nordic Seas on both time scales. The FSB is positively correlated with a regional pattern around Svalbard and northern Barents Sea on interannual timescales.

After 3 months, this anomaly is seen to occupy the area from BSO and along the FSB (being significant at the BSO). After 6 months, interestingly, the core of the warm anomaly is located at depths between 200 and 300 m, but the entire water column down to 600 m shows a warming. After 9–12 months the warm temperature anomaly is predominantly located along the FSB, and has a vertical extent from the surface down to about 300 m. A cross-correlation analysis between the FSB temperature (0–300 m averaged) and SvB transport shows an increasing positive correlation with a maximum at a lag of 9–12 months, which is consistent with the findings in Figure 11 (cf. supporting information Figure S4). It is also interesting to note that the apparent propagation speed of the anomalies is much faster during the first 2–3 months. Thereafter, it becomes rather slow along the BSO and the FSB, where it shows a clear amplification. This is a surprising finding, since one would have expected a cooling and not a warming as the anomaly moves poleward.

6.1.1. Into the Lofoten Basin Interior

We begin by highlighting the importance of the eddies in the LB. Figure 12 examines the eddy kinetic energy ($EKE = \frac{1}{2}(\frac{g}{f}\nabla SLA)^2$) structure that emerges when decomposing it (Figure 12a) into low-frequency (Figure 12b) and high-frequency (Figure 12c) parts, as this is useful in separating the EKE related to the mean flow (LF-EKE) from mesoscale eddies or meanders (HF-EKE). In general, the EKE is high along the

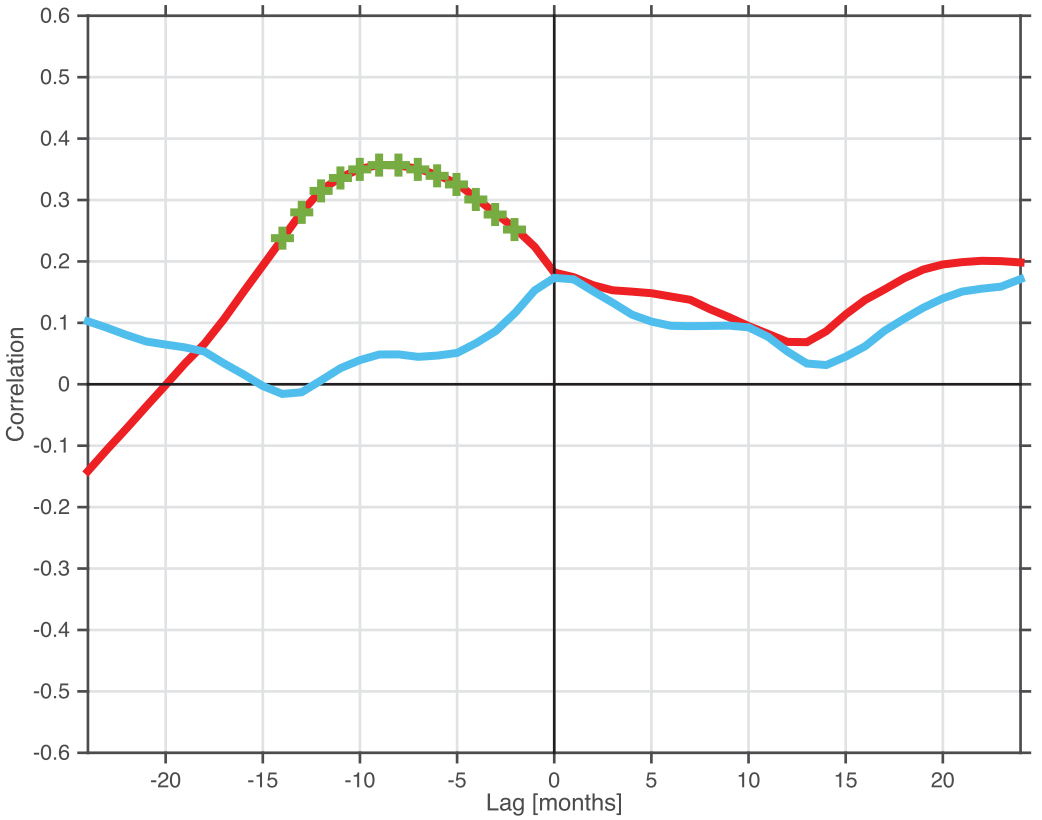

Figure 10. Cross-correlation of the NAO with the SvB (red) and FSB (blue) transport proxy on interannual timescales. The time series have been filtered with 1 year running mean. The green plus signs indicate significant correlations at the 95% confidence level ($p < 0.05$).

domain occupied by Atlantic water in the Nordic Seas, where, however, the most intense eddy activity is found within the interior of the LB. Two pronounced EKE maxima stand out in the LB; offshore the continental slope and in the centre of the basin. The HF-EKE dominates over the LF-EKE, indicating that mesoscale eddies are populating the entire basin, while the LF-EKE dominates the Lofoten escarpment. This feature is, however, suppressed in the HF domain. Instead, the HF-EKE demonstrates a conspicuous increase offshore and toward the interior of the Basin when compared with the LF-EKE, as highlighted by the difference between HF- and LF-EKE shown in Figure 12d. This indicates that mesoscale eddies account for a large fraction of the total EKE. These eddies are shed persistently from the slope current and drift into the LB interior (see the supporting information animation) [*Isachsen*, 2015; *Raj et al*., 2015; *Søiland and Rossby*, 2013; *Koszalka et al*., 2011; *Rossby et al*., 2009a; *Köhl*, 2007].

Figure 13 shows the evolution of composite temperature anomalies in the Lofoten Basin. Also here, the composite anomaly is constructed from time instances with anomalously strong SvB transport. In general, the composite anomaly is warm in the top 500 m and cold in the lower 500–1000 m. The temperature composite thus has a baroclinic signature. At zero lag, both the warm and cold anomaly extend into the Basin. The cold anomaly at around 4°E shows a bowl-shaped structure, which could be an effect of the semipermanent Lofoten vortex residing here [*Raj et al*., 2015; *Köhl*, 2007] over the deepest part of the LB. At a lag of 2 months, a signal extending from the continental slope appears to migrate into the LB with a slight amplification. The cold lower anomaly, i.e., between 500 and 1000 m, now shows now a double convex lens structure due to the vortex, distinguished by the upward and downward sloping isotherms [*Raj et al*., 2015; *Søiland and Rossby*, 2013; *Rossby et al*., 2009b; *Köhl*, 2007]. At a lag of 3–6 months, the warm composite anomaly has shifted westward toward the LB interior, slightly intensifying its amplitude at 9 months, and almost doubling it at 12 months as it reaches the deepest part of the Basin. Assuming that the composite analysis reveals spatial propagation of the temperature anomalies, the anomaly speed can visually be estimated to be around 1.5 km/d (calculated as 500–600 km/365 days), which is in line with the estimated speed ranges for barotropic topographic Rossby waves in the Lofoten Basin [*Volkov et al*., 2013]. Thus, there

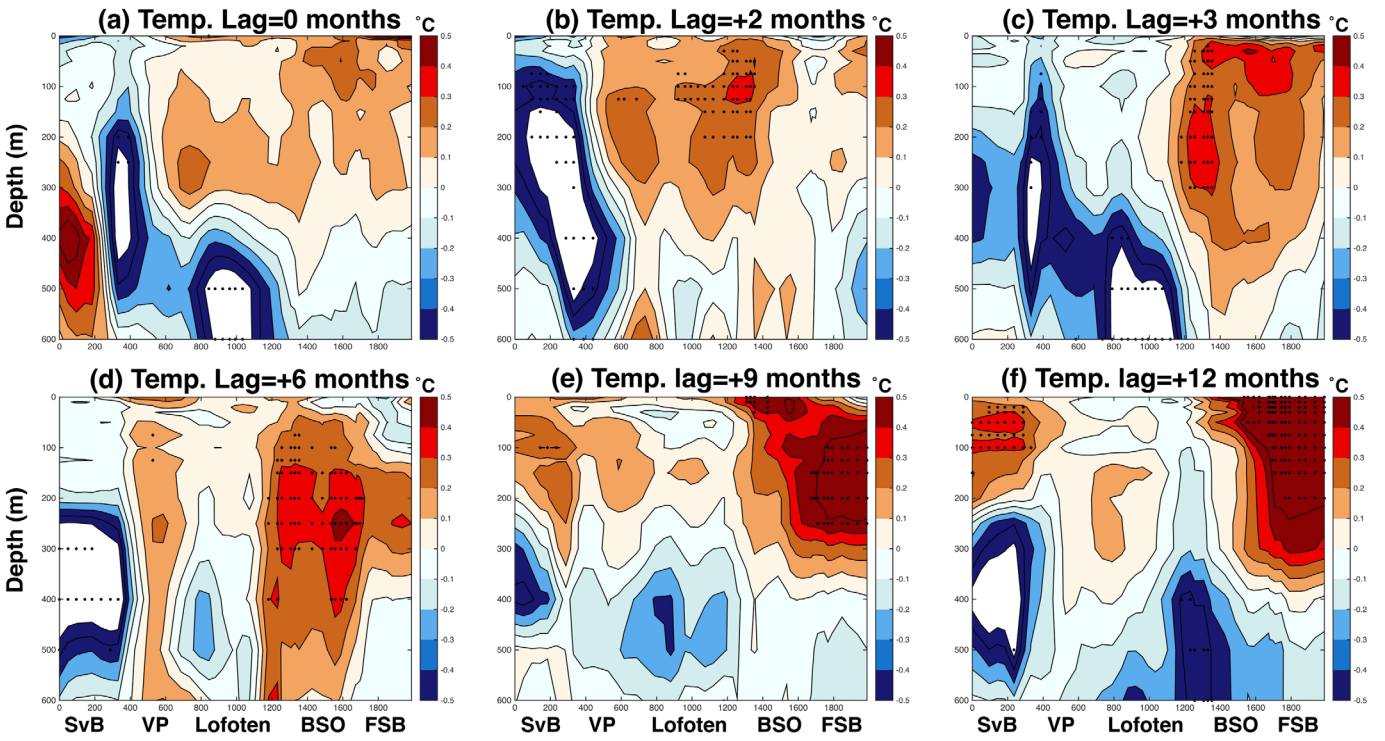

Figure 11. Time Lag composite analysis (depth-distance) of the temperature anomaly, in °C, following the main core of Atlantic water (cf. supporting information Figure S1) in the Nordic Seas and toward the Fram Strait. The composite is based on SvB transport proxy events, defined as months exceeding 1 standard deviation. Positive lags are evaluated at (a) zero-lag, (b) 2 months. (c) 3 months, (d) 6 months, (e) 9 months, and (f) 12 months. Black stipplings represent grid points that are significant at the 95% confidence level ($p < 0.05$) assessed based on a two-sided t-test. The regions are invoked to simplify the orientation along the NwASC (cf. Figure 1). The temperature anomaly is found around Lofoten at 2 months, and later along BSO and FSB, where it is amplified.

appears to be a degree of consistency between the propagation of composite temperature anomalies (Figure 13), the propagation of eddy- and wave-features in the Lofoten Basin seen in altimetry, and Lagrangian data [*Raj et al*., 2015; *Volkov et al*., 2013; *Koszalka et al*., 2013; *Rossby et al*., 2009b; *Köhl*, 2007].

7. Discussion

7.1. Along-Stream Variations of the Flow

Focusing initially on the time-mean barotropic transport measure, we note that it shows along-stream variations of nearly a factor of 4. This is not expected for an inviscid equivalent barotropic geostrophic flow, which conserves the planetary potential vorticity. Ignoring the variations in f, conservation of planetary potential vorticity for a barotropic or an equivalently barotropic flow implies that for steady flow $\mathbf{u} \cdot \nabla H = 0$, i.e., the flow is directed along the isobaths [e.g., *LaCasce and Isachsen*, 2010]. If this was the case, then the time-mean volume transport would be invariant between any two isobaths. There are several possible reasons for why the present simplistic time-mean volume transport indicator varies along stream:

1. The geoid estimate may be inaccurate [*Johannessen et al*., 2014], and/or the resolution of the gridded SSH may be inadequate to resolve the steepest parts of the slope.
2. The flow is not equivalently barotropic and there are along-stream buoyancy gradients (see supporting information Figure S5) that give rise to cross-isobath volume transports, even if the bottom flow is essentially aligned with the bathymetry.
3. For nonzero Rossby numbers, conservation of potential vorticity may cause the flow to make excursions across the isobaths: In the barotropic inviscid limit, $(\zeta + f)/H$ is conserved along the stream lines, where ζ is the relative vorticity. To the lowest order in the Rossby number on an f plane, the flow is completely aligned with the bathymetry. As a consequence, there will be along-stream changes in relative vorticity where the isobaths curve, diverge or converge. For nonzero Rossby numbers, cross-isobath excursion of the stream-lines are dictated by the conservation of potential vorticity: where the relative vorticity

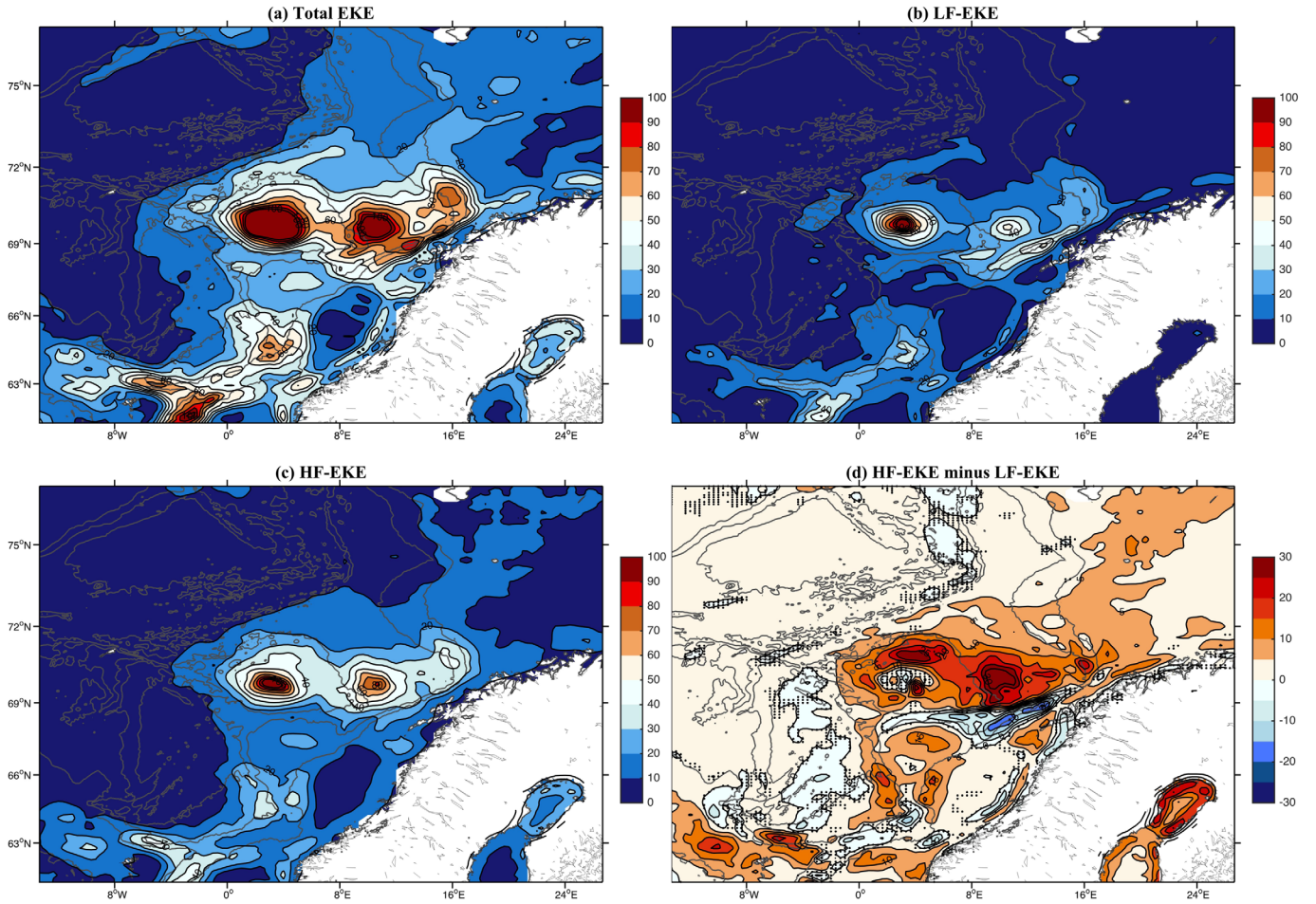

Figure 12. The spatial pattern of the time-averaged (1992–2012) filtered eddy kinetic energy (cm^2s^{-2}) for the Nordic Seas: (a) The total EKE (no-filtering applied), (b) its low-frequency (LF-EKE), and (c) its high-frequency (HF-EKE) part. Note The difference between the HF-EKE (Figure 12c) and the LF-EKE (Figure 12b), and stipplings indicate the differences that are significant at 95% confidence level. The gray lines are the 1000, 2000, and 3000 m bathymetric contours. The Lofoten slope is characterized by LF-EKE and not exposed to the eddies (HF-EKE), while the interior of the LB is dominated by the HF-EKE variability.

increases down-stream, the stream-lines will veer toward deeper water. It is straightforward to show that [e.g., *Nøst et al.*, 2008]

$$\delta H/H \approx \delta\zeta/f, \tag{9}$$

where δH is the first-order stream-line depth correction and $\delta\zeta$ the change in the zero-order relative vorticity along the isobath.

4. Wind-forced or bottom friction related Ekman pumping/suction induce cross-isobath geostrophic flow, which may be viewed as a topographic Sverdrup balance [*Skagseth*, 2004].

We also note that the time-mean transport indicator tends to increase where the slope is steeper and the continental shelf is narrower, which indicate that the local increases of the transport indicator may reflect nonlinear effects and/or confluence of transport from shallower and more gently sloping waters, where the topographic steering is weaker.

We conclude this discussion by providing a rough estimate of how large along-stream isobath transport variations that can be expected to arise from along-stream buoyancy variations and cross-isobath excursions due to conservation of potential vorticity. The changes in steric height, say $\delta\eta_s$, along the NwASC are on the order of 0.08 m, with anomalously high steric height encountered around 64° and 70° N; see supporting information Figure S5. Assuming that the associated horizontal buoyancy variations are depth independent, the variations in cross-isobath baroclinic transport is $\frac{gH\delta\eta_s}{2f}$, which calculated on the 700 m isobath gives about 3 Sv. If further $\delta\eta_s$ is constant across a range of isobaths, say ΔH, then the along-isobath variation in

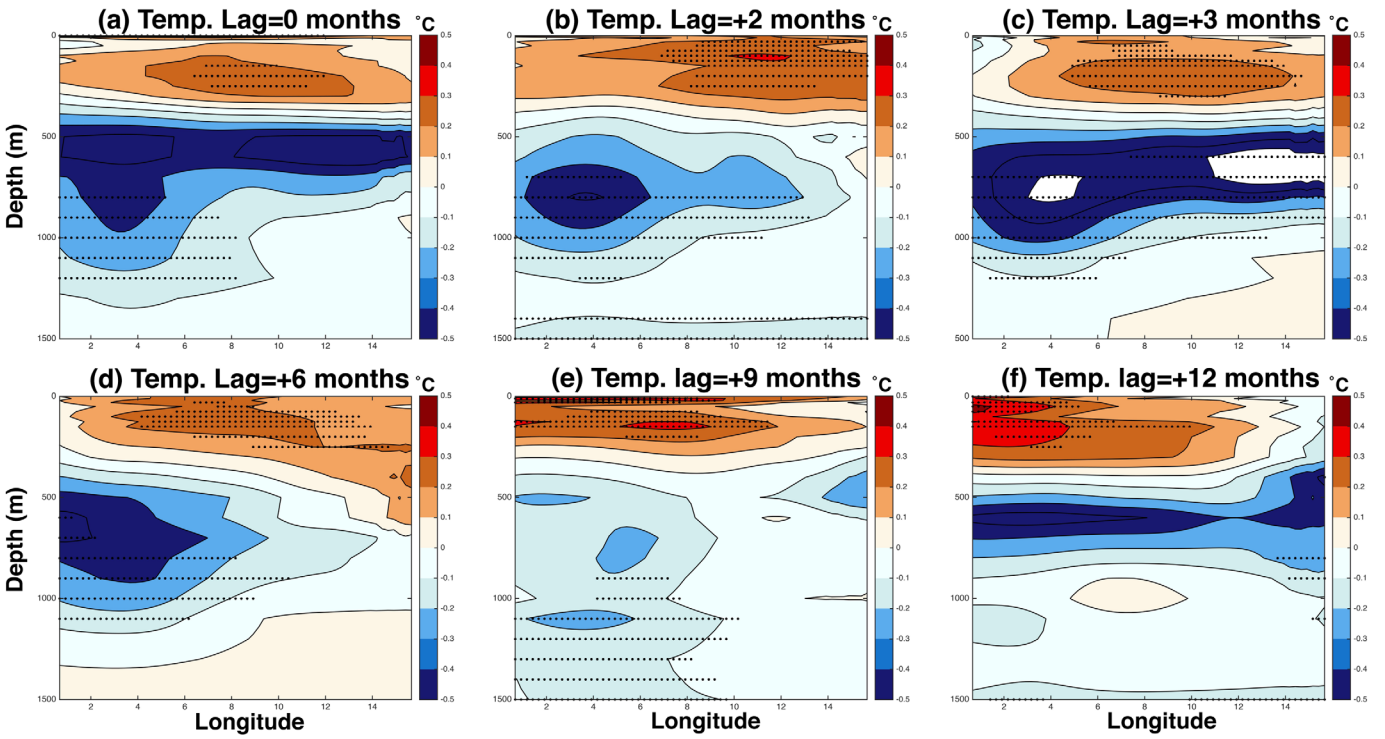

Figure 13. Time Lag composite analysis (depth-distance) of the temperature anomaly, in $^{\circ}C$, following the extension of Atlantic water into the Lofoten Basin (Basin-averaged between 69 and 71°N, cf. Figure 2). The composite is based on SvB transport proxy events, defined as months exceeding 1 standard deviation. Positive lags are evaluated at (a) zero-lag, (b) 2 months. (c) 3 months, (d) 6 months, (e) 9 months, and (f) 12 months. Black stipplings represent grid points that are significant at the 95% confidence level assessed based on a two-sided t-test. The subsurface temperature anomaly propagates westward and amplifies enroute as it reaches the deepest part of the Lofoten Basin, especially at 12 months.

baroclinic transport is approximately $\frac{g\Delta H\delta\eta_s}{2f}$; which is roughly 2 Sv in 500 to 900 m isobath range. These numbers serve as rough upper bounds, since the horizontal buoyancy gradients tend to diminish with depth.

To estimate the effect of potential vorticity conservation, we note that the correction to the transport indicator Ψ, defined by Eqs. (5–7), is obtained by changing the integration limits to $H_1 + \delta H_1$ and $H_2 + \delta H_2$; where the depth changes are given by Eq. (9). If the along-isobath changes in $\delta\zeta$ are approximately constant over the 500 to 900 m isobath range, then the correction to the zero-order along isobath transport Ψ is approximately given by

$$\delta\Psi \approx -2\Psi\delta\zeta/f. \tag{10}$$

Along-isobath variations of ζ/f, computed from the altimetrically derived geostrophic surface velocity field, are on the order of 0.1 (not shown). Taking a mean transport of 2–3 Sv implies that potential vorticity conservation may cause variations of the transport between the 500 to 900 m isobaths of up to 0.5 Sv. This qualitative discussion suggests that some fraction, which could be as large as 1 or 2 Sv, of the variations of our time-mean volume transport indicator along the NwASC may have a dynamical origin. A more quantitative analysis of this issue is, however, beyond the scope of the present work.

7.2. On the Flow Consistency

The instantaneous correlation of the SvB/FSB anomalies with the NwASC have been shown to be weakest north/south of ~70°N. Figure 7 confirmed that the flow anomalies are indeed reduced north of ~70°N. Interestingly, we find no indication of poleward propagating flow anomalies north of this latitude. Plausible mechanisms that could inhibit the structural consistency are discussed. First, we note that along the Norwegian coastal barrier, barotropic along-isobath flow tends to be accelerated by along-slope winds [*Gill and Schumann*, 1974]. However, in the BSO, the NwASC lacks a coastal barrier and there is no direct along-isobath acceleration from winds aligned with the current. Second, the NwASC north of ~70°N is no longer a simple extension of the Atlantic water. The current bifurcates into the Barents Sea, which could impact on

the NwASC consistency. Third, the vigorous and persistent eddy shedding into the LB and the associated-signal transfer into the interior may also damp the consistency of the NwASC. As discussed by *Isachsen et al.* [2012], the Lofoten slope is very steep, dynamically similar to a vertical wall, and hence less capable of stabilizing the flow [see also *Bracco et al.*, 2008]. *Rossby et al.* [2009a] demonstrated that intermediate-depth floats indeed progressed coherently with the NwASC, but turned suddenly westward into the Lofoten Basin (cf. their Figure 10). All these processes are likely to be important, individually or in combination.

The mechanisms described above may explain why the consistency is reduced north of ~70°N, but they do not explain why the correlation drops over VP and increases again over Lofoten (Figure 6). A simple argument can help to illuminate this: Let us define

$$\langle A \rangle \equiv \frac{1}{t_2 - t_1} \int_{t_1}^{t_2} A \, dt, \tag{11}$$

where $A(t)$ is an arbitrary function. Further, let the signal at an arbitrary point y_0 along the NwASC be $A(t)$ and at a point downstream be $B(y,t) = A(t) + N(y,t)$, where A is a coherent signal and N is taken as stochastic noise with an amplitude that can vary in space. The instantaneous correlation can be written as

$$C_{AB} = \frac{\langle AB \rangle}{\langle A^2 \rangle^{1/2} \langle B^2 \rangle^{1/2}} \tag{12}$$

Suppose that A is fairly coherent but N is white noise, then we have approximately

$$C_{AB} = \frac{\langle A^2 \rangle}{\langle A^2 \rangle^{1/2} \langle A^2 + N^2 \rangle^{1/2}} \tag{13}$$

Thus, as the noise level goes up (down) the correlation decreases (increases). Along the VP, noise or HF-EKE (eddies) clearly contaminate the variability, while the LF-EKE (mean-flow) is dominant along the Lofoten slope (Figure 12d).

7.3. Contrasting the Two Flow Regimes

The relationship between the MSLP/SSH and the transport revealed two distinctly different patterns for SvB and FSB, respectively, on both monthly and interannual timescales. On monthly scales, we find that SvB flow anomalies are associated with an NAO-like pattern (minimum north of Iceland) and a depressed SSH within the Nordic Seas with a transition to positive SSH anomalies on the shelf (cf. Figures 8a and 9a). These MSLP/SSH patterns are consistent with previous findings when using Svinøy current-meter data [*Richter et al.*, 2012; *Skagseth et al.*, 2008, 2004; *Mork and Blindheim*, 2000]. However, the FSB results reported here are novel. In this regard, the FSB flow anomalies show a more northerly extent of the MSLP providing winds along the FSB and corresponding higher SSH along the entire eastern continental shelf and over the Barents Sea (cf. Figures 8c and 9c). A positive MSLP anomaly develops on interannual timescales, which through Ekman transport leads to an anticyclonic circulation (positive SSH) anomaly over the northern Barents Sea and around Svalbard, which enhances the FSB transport (cf. Figures 8d and 9d).

Our results clearly indicate that atmosphere-ocean interactions over the Barents Sea affect the FSB. This is in accordance with *Lien et al.* [2013] reporting that a wind-induced cyclonic circulation anomaly, also over the northern Barents Sea and around Svalbard, enhances the flow through the Barents Sea while weakening the FSB. We note that on interannual timescales, the SSH pattern associated with the SvB (Figure 8b) shows a negative anomaly in the northern Barents Sea. This pattern is similar to that previously described by *Lien et al.* [2013], and should enhance the flow of Atlantic Water into the Barents Sea, thus indicating that on longer time scales an anomalous transport increase of the SvB covaries with an enhanced Barents Sea inflow, suggesting that the atmospheric circulation driving these flows is indeed similar. This is supported by the findings in *Skagseth et al.* [2008], which, using current-meter data demonstrated that Svinøy and Barents Sea inflow transports are strongly correlated and dominated by the same atmospheric variability or storm tracks. Our approach of separating between the SvB and FSB is valuable, and shows that on monthly to interannual timescales the atmospheric patterns and hence the induced ocean circulation anomalies differ between these branches. We propose that a regional pattern encircling Svalbard is capable of regulating the FSB and hence the Atlantic inflow to the Arctic.

7.4. Poleward Propagating Warm Anomalies

A number of studies have reported on the propagation of hydrographic anomalies in the Nordic Seas [*Yashayaev and Seidov*, 2015; *Glessmer et al*., 2014; *Lien et al*., 2014; *Koszalka et al*., 2013; *Holliday et al*., 2008; *Sundby and Drinkwater*, 2007; *Polyakov et al*., 2005; *Furevik*, 2001; *Gerdes and Köberle*, 1999]. However, with the exception of *Sundby and Drinkwater* [2007] who argued that NAO strengthened circulation would create positive salinity anomalies in the Norwegian Atlantic current, little evidence has been presented that connects changes in transport and hydrography. Our findings demonstrate a strong link between temperature anomalies and the transport in the Nordic Seas (Figures 11 and 13), and the basic underlying idea is tied to the fact that the temperature along the NwASC gradually decreases downstream: the mean flow advection balances heat loss to the atmosphere and that due to eddy-flux divergence. By linearizing the temperature-advection equation one obtains:

$$\frac{\partial T'}{\partial t} + v' \frac{\partial \bar{T}}{\partial y} + \bar{v} \frac{\partial T'}{\partial y} = R', \tag{14}$$

where the primes and the overbars denote perturbations and mean state, respectively; and R′ additional linear processes. As the temperature gradient is negative (colder downstream), a positive velocity perturbation act to create a positive temperature perturbation. This suggests a positive correlation between velocity and temperature perturbations. However, there are instances when other processes may dominate and change the nature of the correlation. Baroclinic eddies, for instance, can presumably be associated with velocity and temperature perturbations of different signs. However, the time-scale associated with a passing baroclinic eddy is relatively short. Another relevant example is where the flow perturbation is created by a local increase in the along coast wind (quasi northward). In this cases, the temperature perturbations may be dominated by Ekman advection, vertically as well as across the stream. The cross-stream Ekman advection tends to cool whereas the near-coast downwelling tends to warm. It is possible that the cooling effect dominates in some situations and the warming effect in others. These considerations support the notion that there in most cases should be a positive correlation between perturbations in temperature and flow speed, but are they linked to the NAO? Figure 14 looks into the NAO-SvB transport relationship. We note that positive anomalies larger than 1 standard deviation of the SvB transport do not always coincide with positive NAO conditions, while more than 80% of the anomalies larger than 1.5 standard deviation fall within positive NAO conditions. Thus, for extreme positive transport anomalies, i.e., higher than 1.5 standard deviation, the role of the large-scale atmospheric circulation is more important. The local winds and the passage of low-pressure systems may be more effective in generating SvB transport anomalies larger than 1 standard deviation [*Lien et al*., 2014; *Richter et al*., 2009].

It was quite surprising to find that the warm anomaly propagated much faster between Svinøy and BSO as compared to the BSO and FSB distance. It traversed the Svinøy-BSO distance in about 3 months, which corresponds to a speed of about ∼0.15 m/s (1200 km in 3 months). While for the BSO-FSB, we roughly estimate the speed to be ∼0.035 m/s (800 km in 9 months), which is about 4 times slower than the speed recorded between Svinøy and BSO. *Yang and Pratt* [2012] showed using an idealized Nordic Seas that a baroclinic Kelvin wave has a speed of 0.91 m/s and will take around 40 days to travel around the rim of the Nordic Seas. Hence, our speeds are too slow to be linked to this baroclinic Kelvin wave.

Climatologically, this difference in the speed between the Norwegian continental slope and north of it is also exist in the surface velocities (see supporting information Figure S6), and reflected in the transport proxy of the NwASC (cf. Figure 3). The surface current along the NwASC has a speed of 0.2 m/s along the continental slope of Norway, about 0.08–0.1 m/s at the BSO, and 0.1–.12 m/s along the FSB. *Lien et al*. [2014] found that positive salinity anomalies from Svinøy to the BSO during the 2000s propagated at a speed of 0.17 m/s, while between BSO (20°E,72°N) and Vardø (30°E, 70–74°N) the speed was as low as 0.04 m/s, however, no explanation was given for this difference in the propagation speeds. Based on drifter data, *Koszalka et al*. [2013] pointed out that the mean velocity is not constant in the Nordic Seas, and that it is largest in the Norwegian Sea and and drops to 0.04 m/s north of the Lofoten Basin. We also note a clear amplification and surface intensification of the warm anomaly as its speed changed at the BSO and especially along the FSB during its last 9–12 months. Plausibly, the amplification is an effect of the temperature convergence due to a changing and dampened propagation speed. It is also worth noting that in the BSO region where the Atlantic Water fractionates, the temperature gradient changes from being mainly cross-

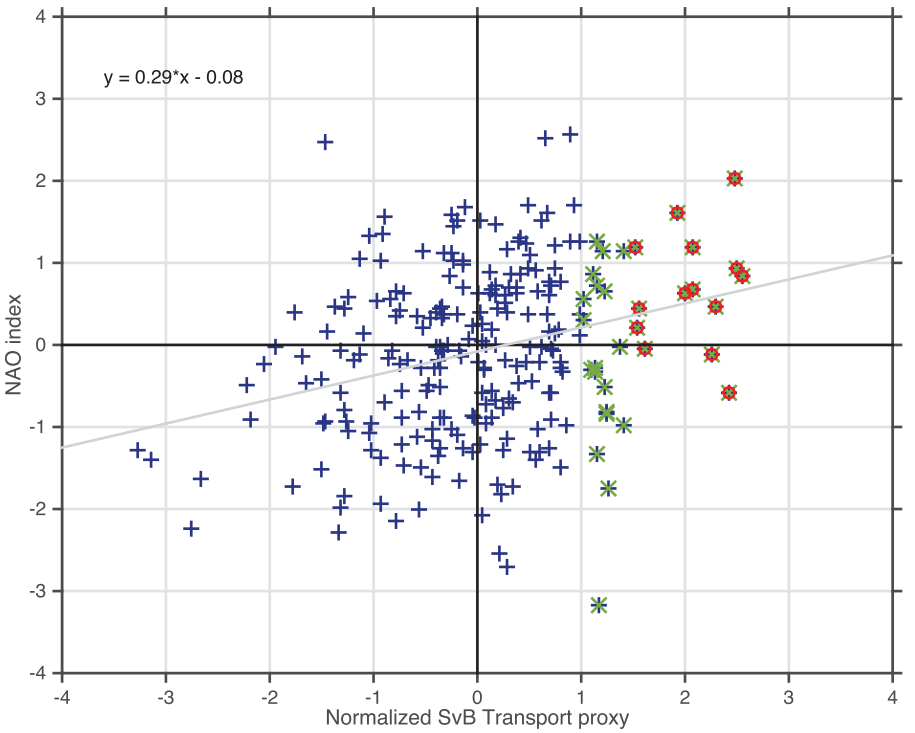

Figure 14. The Normalized SvB transport months versus monthly North Atlantic Oscillation index (obtained from *http://www.cpc.ncep.noaa.gov*) during 1992–2012 period (blue plus signs). Their regression line (in gray) and the corresponding equation are also shown. The correlation $R^2 = 0.08$. Green crosses show all events of the SvB transport that exceed 1 standard deviation. Red circles show events exceeding 1.5 standard deviation, which are found to mostly fall within the positive phase quadrant of the NAO index. Note that extreme SvB transport events (red circles) can be related to positive NAO.

flow to mainly along-flow (cf. Figure 2). Hence, a dynamically driven temperature anomaly propagating downstream, as described by *Sundby and Drinkwater* [2007], would be expected to amplify in this region as the along-flow gradient is pushed downstream.

Based on Eq. (14) it is obvious that a propagating velocity perturbation (e.g., a barotropic topographic shelf wave) creates a larger temperature perturbation where the along-stream mean temperature gradient is greater. There is even a possibility that a downstream decreasing mean temperature can amplify baroclinic anomalies that have a positive correlation between temperature and velocity. Consider a local warm perturbation in the NwASC: if the regions further seaward of the NwASC have essentially an undisturbed temperature, then the warm temperature anomaly will locally give a positive perturbation in the thermal wind, i. e. $v' \sim T'$. From the same equation it follows that there is a tendency for the perturbation to amplify exponentially as it propagates and that the amplification rate is proportional to the (negative) along-stream mean temperature gradient. However, counteracting perturbations in eddy-flux divergence and air-sea heat fluxes are likely to be strong enough to limit the amplitude of the temperature perturbations. Nevertheless, this very qualitative reasoning suggests that anomalies propagating along the NwASC may cause larger temperature perturbations where the along-stream mean temperature gradient is greater.

The warm temperature anomaly routed into the LB interior is an interesting finding, since hitherto, only eddies and drifters/floats have been tracked to target the LB [*Raj et al*., 2015; *Volkov et al*., 2013; *Koszalka et al*., 2013; *Rossby et al*., 2009a]. Most recently, *Raj et al*. [2015] show that these eddies, which originate at the Lofoten escarpment, are likely to merge with the quasi-permanent Lofoten vortex, a process that increases the vorticity of the Lofoten vortex. We argue that a similar process may have intensified the observed westward propagating warm anomaly as it reached the LB interior (Figure 13), where the vortex resides. Hence, the quasi-permanency of the Lofoten eddy may in part be due to the persistent eddy shedding (see the supporting information animation) and merging of warm anomalies from the NwASC. Our results suggest that the composite temperature anomaly is consistent with the notion that eddies carry and deposit warm Atlantic water in the interior of the Lofoten Basin. The increased persistence of anomalous

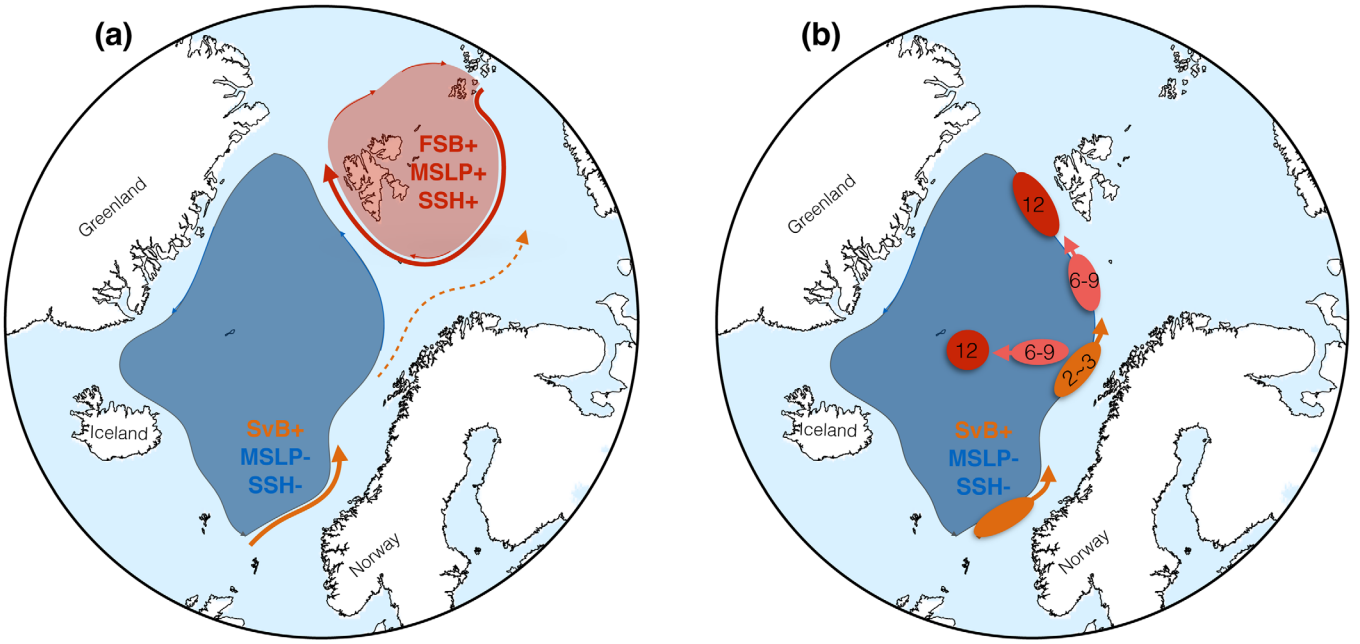

Figure 15. Schematic diagrams of the main findings. (a) The MSLP/SSH patterns driving the SvB and the FSB, respectively. The SvB is associated with a negative MSLP/SSH anomaly within the Nordic Seas, which is likely to influence the Barents Sea inflow as well. The FSB is linked to a positive MSLP/SSH anomaly around Svalbard and northern Barents Sea. (b) The propagation of warm temperature anomalies into the LB and toward the Fram Strait. The SvB+ here points out that these anomalies are related to anomalous positive transport events recorded at the SvB. The arrows indicate the direction of the temperature anomaly, the colors display that the anomaly intensifies enroute, and the numbers are the approximate transit times.

heat content in the centre of the LB (with a significant autocorrelation at 1 year lag) shown by *Skagseth and Mork* [2012] supports this view.

8. Concluding Remarks

Resolving the spatio-temporal variability of the NwASC transport gave credence to a separation of the flow into two dynamical regimes, i.e., the SvB and FSB, respectively.

On monthly to interannual timescales, the SvB responds strongly to the SSH within the Nordic Seas (Figure 15a). The wind field within the Norwegian Sea is likely to be the important factor for the SvB transport variability, but also for variations of the inflow to the Barents Sea. One possible reason for this coupling may be due to the fact that atmospheric cyclones passing the Norwegian Sea mostly progress into the Barents Sea, thereby accelerating both branches. Therefore, these warm water pathways are sensitive to changes in the storm tracks, a similar point was made by *Lien et al*. [2013].

The variability of the FSB is influenced by wind-induced Ekman transport centered around Svalbard and northern Barents Sea (Figure 15a). Thus, the fractionation of Atlantic water transport toward the Arctic between the Fram Strait and Barents Sea branches is largely modulated by regional atmospheric patterns while the NAO plays a negligible role. Based on the proposed mechanism, a good proxy may simply include the use of SSH from altimetry along with regional atmospheric pressure variations.

The Lofoten Basin is a" hot-spot" for mesoscale eddies. These are found to carry and deposit warm Atlantic water anomalies in the LB interior after they deviate from the NwASC (Figure 15b). Thus, to represent the transport of Atlantic Water to the Arctic in climate models, realistic eddy fluxes and the accompanying volume of Atlantic Water in the Lofoten Basin are prerequisites.

The composite warm anomaly reaching the FSB at roughly 12 months is generated after anomalous transport events in the southern Norwegian Sea (Figure 15b). To the best of our knowledge, little evidence has been presented that connects changes in the transport and hydrography. As a final remark we believe that the combination of SvB transport, either using altimetry or current-meter data, and temperature fluctuations in the Nordic Seas can be used to qualitatively predict warm anomalies toward the Arctic Ocean, which could be a valuable addition to the forecast skill of the statistical Arctic sea-ice models [see e.g., *Lindsay et al*., 2008].

Acknowledgments
The work herein is supported by a grant from the NOAA Jason altimetry program. Johan Nilsson acknowledges support from the Swedish Space Science Board (SNSB). The current-meter data were obtained during the IPY 2007 through the NFR-funded project iAOOSNorway. Thanks to two anonymous reviewers for valuable comments that improved the paper. The authors thank Kjell Arild Orvik for generously providing the long-term transport from the Svin{\o}y section. Laurence Miller is greatly acknowledged for the constructive comments that improved the manuscript. The satellite-altimetry data set, denoted SSALTO/DUACS (multimission ground Segment for ALTimetry, Orbitography and precise localisation/Developing Use of Altimetry for Climate Studies), was obtained courtesy of the French archive AVISO (Archiving, Validation and Interpretation of Satellite Oceanographic Data, http:// www.aviso.oceanobs.com).

References

Aaboe, S., and O. A. Nøst (2008), A diagnostic model of the Nordic Seas and Arctic Ocean circulation: Quantifying the effects of a variable bottom density along a sloping topography, *J. Phys. Oceanogr.*, *38*(12), 2685–2703, doi:10.1175/2008JPO3862.1.

Andersson, M., K. A. Orvik, J. H. LaCasce, I. Koszalka, and C. Mauritzen (2011), Variability of the Norwegian Atlantic Current and associated eddy field from surface drifters, *J. Geophys. Res.*, *116*, C08032, doi:10.1029/2011JC007078.

Årthun, M., T. Eldevik, L. H. Smedsrud, Ø. Skagseth, and R. B. Ingvaldsen (2012), Quantifying the influence of Atlantic heat on Barents Sea ice variability and retreat, *J. Clim.*, *25*(13), 4736–4743, doi:10.1175/JCLI-D-11-00466.1.

Beszczynska-Möller, A., E. Fahrbach, U. Schauer, and E. Hansen (2012), Variability in Atlantic water temperature and transport at the entrance to the Arctic Ocean, 1997–2010, *ICES J. Mar. Sci. 69*, 852–863, doi:10.1093/icesjms/fss056.

Björk, G., B. Gustafsson, and A. Stigebrandt (2001), Upper layer circulation of the Nordic seas as inferred from the spatial distribution of heat and freshwater content and potential energy, *Polar Res.*, *20*(2), 161–168.

Blindheim, J., V. Borovkov, B. Hansen, S. A. Malmberg, W. R. Turrell, and S. Østerhus (2000), Upper layer cooling and freshening in the Norwegian Sea in relation to atmospheric forcing, *Deep Sea Res., Part I*, *47*(4), 655–680, doi:10.1016/S0967-0637(99)00070-9.

Bracco, A., J. Pedlosky, and R. S. Pickart (2008), Eddy formation near the West Coast of Greenland, *J. Phys. Oceanogr.*, *38*(9), 1992–2002, doi:10.1175/2008JPO3669.1.

Carton, J. A., G. A. Chepurin, J. Reagan, and S. Häkkinen (2011), Interannual to decadal variability of Atlantic Water in the Nordic and adjacent seas, *J. Geophys. Res.*, *116*, C11035, doi:10.1029/2011JC007102.

Chepurin, G. A., and J. A. Carton (2012), Subarctic and Arctic sea surface temperature and its relation to ocean heat content 1982–2010, *J. Geophys. Res.*, *117*, C06019, doi:10.1029/2011JC007770.

Dee, D. P., et al. (2011), The ERA-interim reanalysis: Configuration and performance of the data assimilation system, *Q. J. R. Meteorol. Soc.*, *137*(656), 553–597, doi:10.1002/qj.828.

Drange, H., T. Dokken, T. Furevik, R. Gerdes, W. Berger, A. Nesje, K. Arild Orvik, O. Skagseth, I. Skjelvan, and S. Østerhus (2005), *The Nordic Seas: An Overview*, pp. 1–10, AGU, Washington, D. C., doi:10.1029/158GM02.

Furevik, T. (2001), Annual and interannual variability of Atlantic Water temperatures in the Norwegian and Barents Seas: 1980–1996, *Deep Sea Res., Part I*, *48*(2), 383–404, doi:10.1016/S0967-0637(00)00050-9.

Furevik, T., and J. E. Ø. Nilsen (2005), *Large-Scale Atmospheric Circulation Variability and its Impacts on the Nordic Seas Ocean Climate—A Review*, pp. 105–136, AGU, Washington, D. C., doi:10.1029/158GM09.

Gerdes, R., and C. Köberle (1999), Numerical simulation of salinity anomaly propagation in the Nordic Seas and the Arctic Ocean, *Polar Res.*, *18*(2), 159–166.

Gill, A. E., and E. H. Schumann (1974), The generation of long shelf waves by the wind, *J. Phys. Oceanogr.*, *4*(1), 83–90, doi:10.1175/1520-0485(1974)004¡0083:TGOLSW¿2.0.CO;2.

Glessmer, M. S., T. Eldevik, K. Vage, J. E. Oie Nilsen, and E. Behrens (2014), Atlantic origin of observed and modelled freshwater anomalies in the Nordic seas, *Nat. Geosci.*, *7*(11), 801–805.

Gordon, R. L., and J. M. Huthnance (1987), Storm-driven continental shelf waves over the Scottish continental shelf, *Cont. Shelf Res.*, *7*(9), 1015–1048, doi:10.1016/0278-4343(87)90097-5.

Häkkinen, S., and P. B. Rhines (2004), Decline of subpolar North Atlantic Circulation during the 1990s, *Cont. Shelf Res.*, *304*(5670), 555–559.

Häkkinen, S., P. B. Rhines, and D. L. Worthen (2011), Warm and saline events embedded in the meridional circulation of the northern North Atlantic, *J. Geophys. Res.*, *116*, C03006, doi:10.1029/2010JC006275.

Hansen, B., and S. Østerhus (2000), North Atlantic–Nordic Seas exchanges, *Prog. Oceanogr.*, *45*(2), 109–208, doi:10.1016/S0079-6611(99)00052-X.

Hátún, H., A. B. Sandø, H. Drange, B. Hansen, and H. Valdimarsson (2005), Influence of the Atlantic subpolar gyre on the thermohaline circulation, *Science*, *309*(5742), 1841–1844.

Holliday, N. P., et al. (2008), Reversal of the 1960s to 1990s freshening trend in the northeast North Atlantic and Nordic Seas, *Geophys. Res. Lett.*, *35*, L03614, doi:10.1029/2007GL032675.

Hurrell, J. W. (1995), Decadal trends in the North Atlantic oscillation: Regional temperatures and precipitation, *Science*, *269*(5224), 676–679, doi:10.1126/science.269.5224.676.

Isachsen, P. E. (2015), Baroclinic instability and the mesoscale eddy field around the Lofoten Basin, *J. Geophys. Res. Oceans*, *120*, 2884–2903, doi:10.1002/2014JC010448.

Isachsen, P. E., J. H. LaCasce, C. Mauritzen, and S. Häkkinen (2003), Wind-driven variability of the large-scale recirculating flow in the Nordic Seas and Arctic Ocean, *J. Phys. Oceanogr.*, *33*(12), 2534–2550.

Isachsen, P. E., I. Koszalka, and J. H. LaCasce (2012), Observed and modeled surface eddy heat fluxes in the eastern Nordic Seas, *J. Geophys. Res.*, *117*, C08020, doi:10.1029/2012JC007935.

Jakobsen, P. K., M. H. Ribergaard, D. Quadfasel, T. Schmith, and C. W. Hughes (2003), Near-surface circulation in the northern North Atlantic as inferred from Lagrangian drifters: Variability from the mesoscale to interannual, *J. Geophys. Res.*, *108*(C8), 3251, doi:10.1029/2002JC001554.

Johannessen, J. A., et al. (2014), Toward Improved Estimation of the Dynamic Topography and Ocean Circulation in the High Latitude and Arctic Ocean: The importance of GOCE, *Surv. Geophys.*, *35*(3), 661–679, doi:10.1007/s10712-013-9270-y.

Killworth, P. D. (1992), An equivalent-barotropic mode in the fine resolution Antarctic Model, *J. Phys. Oceanogr.*, *22*(11), 1379–1387, doi:10.1175/1520-0485(1992)022¡1379:AEBMIT¿2.0.CO;2.

Koenigk, T., and L. Brodeau (2014), Ocean heat transport into the arctic in the twentieth and twenty-first century in ec-earth, *Clim. Dyn.*, *42*(11-12), 3101–3120, doi:10.1007/s00382-013-1821-x.

Köhl, A. (2007), Generation and stability of a quasi-permanent vortex in the Lofoten Basin, *J. Phys. Oceanogr.*, *37*(11), 2637–2651, doi:10.1175/2007JPO3694.1.

Korablev, A. A., A. Smirnov, and O. K. Baranova (2014), Climatological Atlas of the Nordic Seas and Northern North Atlantic, in *NOAA Atlas NESDIS 77*, edited by D. Seidov and A. R. Parsons, 122 pp., doi:10.7289/V5K64G16.

Koszalka, I., J. H. LaCasce, M. Andersson, K. A. Orvik, and C. Mauritzen (2011), Surface circulation in the Nordic Seas from clustered drifters, *Deep Sea Res., Part I*, *58*(4), 468–485, doi:10.1016/j.dsr.2011.01.007.

Koszalka, I., J. H. LaCasce, and C. Mauritzen (2013), In pursuit of anomalies—Analyzing the poleward transport of Atlantic Water with surface drifters, *Deep Sea Res., Part II*, *85*, 96–108, doi:10.1016/j.dsr2.2012.07.035.

LaCasce, J. H., and P. E. Isachsen (2010), The linear models of the acc, *Prog. Oceanogr.*, *84*(3–4), 139–157, doi:10.1016/j.pocean.2009.11.002.

Lien, V., Y. Gusdal, and F. Vikebø (2014), Along-shelf hydrographic anomalies in the Nordic Seas (1960–2011): Locally generated or advective signals?, *Ocean Dyn.*, *64*(7), 1047–1059, doi:10.1007/s10236-014-0736-3.
Lien, V. S., F. B. Vikebo, and O. Skagseth (2013), One mechanism contributing to co-variability of the Atlantic inflow branches to the Arctic, *Nat. Commun.*, *4*, 1488.
Lindsay, R. W., J. Zhang, A. J. Schweiger, and M. A. Steele (2008), Seasonal predictions of ice extent in the Arctic Ocean, *J. Geophys. Res.*, *113*, C02023, doi:10.1029/2007JC004259.
Mork, K. A., and J. Blindheim (2000), Variations in the Atlantic inflow to the Nordic Seas, 1955–1996, *Deep Sea Res., Part I*, *47*(6), 1035–1057, doi:10.1016/S0967-0637(99)00091-6.
Mork, K. A., Ø. Skagseth, V. Ivshin, V. Ozhigin, S. L. Hughes, and H. Valdimarsson (2014), Advective and atmospheric forced changes in heat and fresh water content in the Norwegian sea, 1951–2010, *Geophys. Res. Lett.*, *41*, 6221–6228, doi:10.1002/2014GL061038.
Nøst, O. A., and P. E. Isachsen (2003), The large-scale time-mean ocean circulation in the Nordic Seas and Arctic Ocean estimated from simplified dynamics, *J. Mar. Res.*, *61*(2), 175–210.
Nøst, O. A., J. Nilsson, and J. Nycander (2008), On the Asymmetry between Cyclonic and Anticyclonic Flow in Basins with Sloping boundaries, *J. Phys. Oceanogr.*, *38*(4), 771–787, doi:10.1175/2007JPO3714.1.
Orvik, K. A., and P. Niiler (2002), Major pathways of Atlantic water in the northern North Atlantic and Nordic Seas toward Arctic, *Geophys. Res. Lett.*, *29*(19), 1896, doi:10.1029/2002GL015002.
Orvik, K. A., and Ø. Skagseth (2003a), Monitoring the Norwegian Atlantic slope current using a single moored current meter, *Cont. Shelf Res.*, *23*(2), 159–176, doi:10.1016/S0278-4343(02)00172-3.
Orvik, K. A., and Ø. Skagseth (2003b), The impact of the wind stress curl in the North Atlantic on the Atlantic inflow to the Norwegian Sea toward the Arctic, *Geophys. Res. Lett.*, *30*(17), 1884, doi:10.1029/2003GL017932.
Orvik, K. A., Ø. Skagseth, and M. Mork (2001), Atlantic inflow to the Nordic Seas: Current structure and volume fluxes from moored current meters, VM-ADCP and SeaSoar-CTD observations, 1995–1999, *Deep Sea Res., Part I*, *48*(4), 937–957.
Polyakov, I. V., et al. (2005), One more step toward a warmer Arctic, *Geophys. Res. Lett.*, *32*, L17605, doi:10.1029/2005GL023740.
Poulain, P. M., A. Warn-Varnas, and P. P. Niiler (1996), Near-surface circulation of the Nordic seas as measured by Lagrangian drifters, *J. Geophys. Res.*, *101*, 18,237–18,258, doi:10.1029/96JC00506.
Rahmstorf, S. (1999), Shifting seas in the greenhouse?, *Nature*, *399*(6736), 523–524.
Raj, R. P., L. Chafik, J. E. Ø. Nilsen, T. Eldevik, and I. Halo (2015), The Lofoten vortex of the Nordic seas, *Deep Sea Res., Part I*, *96*, 1–14, doi:10.1016/j.dsr.2014.10.011.
Richter, K., T. Furevik, and K. A. Orvik (2009), Effect of wintertime low-pressure systems on the Atlantic inflow to the Nordic seas, *J. Geophys. Res.*, *114*, C09006, doi:10.1029/2009JC005392.
Richter, K., O. H. Segtnan, and T. Furevik (2012), Variability of the Atlantic inflow to the Nordic Seas and its causes inferred from observations of sea surface height, *J. Geophys. Res.*, *117*, C04004, doi:10.1029/2011JC007719.
Rio, M. H., S. Guinehut, and G. Larnicol (2011), New CNES-CLS09 global mean dynamic topography computed from the combination of GRACE data, altimetry, and in situ measurements, *J. Geophys. Res.*, *116*, C07018, doi:10.1029/2010JC006505.
Rossby, T., M. D. Prater, and H. Søiland (2009a), Pathways of inflow and dispersion of warm waters in the Nordic Seas, *J. Geophys. Res.*, *114*, C04011, doi:10.1029/2008JC005073.
Rossby, T., V. Ozhigin, V. Ivshin, and S. Bacon (2009b), An isopycnal view of the Nordic Seas hydrography with focus on properties of the Lofoten Basin, *Deep Sea Res., Part I*, *56*(11), 1955–1971, doi:10.1016/j.dsr.2009.07.005.
Sandø, A. B., and T. Furevik (2008), Relation between the wind stress curl in the North Atlantic and the Atlantic inflow to the Nordic Seas, *J. Geophys. Res.*, *113*, C06028, doi:10.1029/2007JC004236.
Seidov, D., et al. (2015), Oceanography north of 60°N from World Ocean Database, *Prog. Oceanogr.*, *132*, 153–173, doi:10.1016/j.pocean.2014.02.003.
Skagseth, Ø. (2004), Monthly to annual variability of the Norwegian Atlantic slope current: Connection between the northern North Atlantic and the Norwegian sea, *Deep Sea Res., Part I*, *51*(3), 349–366, doi:10.1016/j.dsr.2003.10.014.
Skagseth, Ø., and K. A. Mork (2012), Heat content in the Norwegian Sea, 1995–2010, *ICES J. Mar. Sci.*, *69*, 826–832.
Skagseth, Ø., and K. A. Orvik (2002), Identifying fluctuations in the Norwegian Atlantic Slope Current by means of empirical orthogonal functions, *Cont. Shelf Res.*, *22*(4), 547–563, doi:10.1016/S0278-4343(01)00086-3.
Skagseth, Ø., K. A. Orvik, and T. Furevik (2004), Coherent variability of the Norwegian Atlantic Slope Current derived from TOPEX/ERS altimeter data, *Geophys. Res. Lett.*, *31*, L14304, doi:10.1029/2004GL020057.
Skagseth, Ø., T. Furevik, R. Ingvaldsen, H. Loeng, K. A. Mork, and V. Ozhigin (2008), *Volume and heat transport to the Arctic Ocean via the Norwegian and Barents Seas, in Arctic - Subarctic Ocean Fluxes*, edited by R. Dickson, J. Meincke, and P. Rhines, pp. 45–64, Springer Verlag, doi:10.1007/978-1-4020-6774-7_3.
Søiland, H., and T. Rossby (2013), On the structure of the Lofoten Basin Eddy, *J. Geophys. Res. Oceans*, *118*, 4201–4212, doi:10.1002/jgrc.20301.
Søiland, H., M. D. Prater, and T. Rossby (2008), Rigid topographic control of currents in the Nordic Seas, *Geophys. Res. Lett.*, *35*, L18607, doi:10.1029/2008GL034846.
Sundby, S., and K. Drinkwater (2007), On the mechanisms behind salinity anomaly signals of the northern North Atlantic, *Prog. Oceanogr.*, *73*(2), 190–202, doi:10.1016/j.pocean.2007.02.002.
Troupin, C., et al. (2012), Generation of analysis and consistent error fields using the Data Interpolating Variational Analysis (DIVA), *Ocean Modell.*, *52–53*, 90–101, doi:10.1016/j.ocemod.2012.05.002.
Volkov, D. L., and M. I. Pujol (2012), Quality assessment of a satellite altimetry data product in the Nordic, Barents, and Kara seas, *J. Geophys. Res. Oceans*, *117*, C03025, doi:10.1029/2011JC007557.
Volkov, D. L., T. V. Belonenko, and V. R. Foux (2013), Puzzling over the dynamics of the Lofoten Basin––A sub-Arctic hot spot of ocean variability, *Geophys. Res. Lett.*, *40*, 738–743, doi:10.1002/grl.50126.
Woollings, T., A. Hannachi, and B. Hoskins (2010), Variability of the North Atlantic eddy-driven jet stream, *Q. J. R. Meteorol. Soc.*, *136*(649), 856–868, doi:10.1002/qj.625.
Yang, J., and L. J. Pratt (2012), On the effective capacity of the dense-water reservoir for the Nordic Seas Overflow: Some effects of topography and wind stress, *J. Phys. Oceanogr.*, *43*(2), 418–431, doi:10.1175/JPO-D-12-087.1.
Yashayaev, I., and D. Seidov (2015), The role of the Atlantic Water in multidecadal ocean variability in the Nordic and Barents Seas, *Prog. Oceanogr.*, *132*, 68–127, doi:10.1016/j.pocean.2014.11.009.
Zhang, J., D. A. Rothrock, and M. Steele (1998), Warming of the Arctic Ocean by a strengthened Atlantic Inflow: Model results, *Geophys. Res. Lett.*, *25*, 1745–1748, doi:10.1029/98GL01299.